Revisiting the relations: Galactic thin disc age–velocity dispersion relation

G. M. Seabroke[★] and G. Gilmore

Institute of Astronomy, University of Cambridge, Madingley Road, Cambridge CB3 0HA

ABSTRACT

The velocity dispersion of stars in the solar neighbourhood thin disc increases with time after star formation. Nordström et al. performed the most recent observations to constrain the age–velocity dispersion relation. They fitted the age–velocity dispersion relations of each Galactic cardinal direction space velocity component, U (towards the Galactic Centre), V (in the direction of Galactic rotation) and W (towards the North Galactic Pole), with power laws and interpreted these as evidence for continuous heating of the disc in all directions throughout its lifetime. We revisit these relations with their data and use the results of Famaey et al. to show that structure in the local velocity distribution function distorts the in-plane (U and V) velocity distributions away from Gaussian so that a dispersion is not an adequate parametrization of their functions. The age–σ_W relation can however be constrained because the sample is well phase-mixed vertically. We do not find any local signature of the stellar warp in the Galactic disc. Vertical disc heating does not saturate at an early stage. Our new result is that a power law is not required by the data: disc heating models that saturate after $\sim$4.5 Gyr are equally consistent with observations.

Key words: galaxy: disc – galaxy: evolution – galaxy: kinematics and dynamics – solar neighbourhood – galaxy: stellar content.

1 INTRODUCTION

The velocity dispersion of the molecular clouds in which star formation is taking place is very much less, by a factor of 3–5, than is the (one-dimensional) dispersion of old stars near the Sun. The (set of) processes which change the velocities in any direction of initially slow-moving young stars into 'hotter', higher dispersion orbits with time are disc 'heating' mechanisms and are evidently fundamental aspects of disc galaxy evolution.

The most recent observational attempt to constrain the age–velocity dispersion relation is by Nordström et al. (2004), hereafter N04, using their Geneva–Copenhagen survey of the solar neighbourhood. This is the largest homogeneous data set available with space velocity components, U (towards the Galactic Centre), V (in the direction of Galactic rotation) and W (towards the North Galactic Pole), and isochrone-derived stellar ages. N04 fitted the age–velocity dispersion relations of each space velocity component (and the total) with continuous smooth power laws: $\sigma \propto \mathrm{age}^k$, where the scaling (heating) exponent, k, is 0.31, 0.34, 0.47 and 0.34 for $\sigma_U, \sigma_V, \sigma_W$ and σ_{total}, respectively. They interpreted these relations as evidence for continuous heating of the disc in all directions throughout its lifetime.

However, continuous vertical (σ_W) heating is unexpected. Stars spend most of their time near the apocentre of their vertical orbits, furthest away from the Galactic plane. For stars to experience con-

tinuous vertical heating throughout their lifetimes requires heating processes that operate away from the plane. Giant molecular clouds (GMCs) gravitationally scatter stars (Spitzer & Schwarzschild 1951, 1953; Lacey 1984; Villumsen 1985; Hänninen & Flynn 2002) but they exist in the extreme thin disc. This suggests that vertical heating should not continue throughout the lifetime of the disc but should saturate after some epoch if GMCs are indeed the primary cause.

There are many heating mechanisms in the literature using non-disc processes to explain continuous vertical heating observations. Lacey & Ostriker (1985) proposed scattering by massive black holes in the halo, which have been simulated by Fuchs, Dettbarn & Wielen (1994) and Hänninen & Flynn (2002). Carr & Lacey (1987) proposed dark clusters of less massive objects could heat stellar discs. However, neither of these major mechanisms have any direct observational support. Minor mergers with dwarf galaxies is another possible heating mechanism (Toth & Ostriker 1992; Walker, Mihos & Hernquist 1996; Huang & Carlberg 1997). Dramatic disc heating can occur when massive satellite galaxies fall on to galactic discs (Quinn, Hernquist & Fullagar 1993), which could leave a sharp feature in the age–σ_W relation but many smaller galaxies accreting could heat a disc smoothly (Velazquez & White 1999). Other possible vertical heating mechanisms that may play a minor role are the outer Lindblad resonance from the Galactic bar (Kalnajs 1991; Dehnen 1999, 2000; Fux 2001; Quillen 2003) and evaporating star clusters (Kroupa 2002). In this paper, we revisit the age–σ_W relation using the same data as N04 to test the uniqueness of their power-law model fit. We investigate whether the data permit models where

[★]E-mail: gs310@ast.cam.ac.uk

the vertical disc heating saturates, thus negating the need to invoke hypothetical or poorly understood components of the Galaxy.

Whether heating is continuous or saturates with time requires separate consideration in the plane (σ_U and σ_V) and out of the plane (σ_W). Simulations by De Simone, Wu & Tremaine (2004) illustrate that transient spiral waves are most likely to be the dominant in-plane heating mechanism in the solar neighbourhood. Transient spiral waves can lead to gravitational potential fluctuations in the disc that excite random motions of disc stars (Barbanis & Woltjer 1967; Sellwood & Carlberg 1984; Carlberg & Sellwood 1985; Sellwood & Binney 2002) but only effectively in U and V because they are confined to the thin disc. GMCs also contribute to the in-plane heating but are unlikely to be the dominant heating source (De Simone et al. 2004). Once a star's epicyclic amplitude reaches a size-scale similar to that of the spiral arm radial wavenumbers, the star will cross more than one spiral arm as it radially oscillates making it more difficult for the spiral structure to perturb it (Carlberg & Sellwood 1985). This means spiral heating is theoretically expected to become much less efficient with time so that its in-plane heating effectively saturates.

However, whether σ_U and σ_V should actually saturate requires simulating the heating from both realistic Galactic spiral structure and GMCs but these calculations are complicated. Spiral features heat a disc at a rate that depends on the spatial pattern of the potential and on its time variability. In principle, the photometry of real galaxies can yield the spatial structures of galaxies and temporal information concerning spiral structure can be determined from numerical simulation and dynamical theory. In practice, the strengths, growth rates and duty cycles of spirals are not well constrained. Therefore, the relative effectiveness of spiral and GMC heating has to be modelled with an empirical parameter (Jenkins & Binney 1990; Jenkins 1992). Naturally, the empirical parameter was guided by observation and so the models reflected the only observationally determined age–velocity dispersion relation of the time (Wielen 1977).

Like N04, Wielen (1977) also found a continuous power law for σ_{total} (and σ_W) with $k \sim 0.5$ but this was based on ranking the age of mainly K and M dwarfs using chromospheric emission-line measurements, which is fraught with systematic errors. Carlberg et al. (1985) used more reliable isochrone ages and found observational evidence for saturation in the age–σ_{total} relation at ages >5 Gyr but this was obtained using tangential velocities and only 255 stars. Quillen & Garnett (2001) argued for earlier saturation in $\sigma_U, \sigma_V, \sigma_W$ and σ_{total} between 3 and 10 Gyr. However, this was based on only 189 Edvardsson et al. (1993) stars (~21 stars per logarithmic age bin) and although they used new improved isochrone ages from Ng & Bertelli (1998), their age determination is less reliable than N04. Also, Stromgren (1987), Freeman (1991) and Gomez et al. (1997) all argued for a turnover in the observational relation, indicative of saturation.

The in-plane heating saturation issue is complex because it is not clear if the observations are reliable and the simulations depend on the observations. In this paper, we argue that this issue is still not observationally resolved even though N04 presented evidence of continuous in-plane heating. We show their analysis is not conclusive because the interpretation of the in-plane age–velocity dispersion relation is complicated by the presence of strong, stellar age-dependent, small-scale structure.

De Simone et al. (2004) demonstrate that heating by strong transient spiral waves can induce strong small-scale structure in the local U and V velocity distributions by imparting momentum to stars to put them in specific regions of the UV plane, creating streams with a stellar age range of ~3 Gyr. Sellwood & Binney (2002) found that spiral waves cause radial migration in the galactic disc near their corotation radius, preserving overall angular momentum leading to only a small increase in random motions. This naturally explains the 'dynamical streams' found in the kinematic survey of local K–M giants by Famaey et al. (2005), hereafter F05, which have similar properties to moving groups and superclusters but which contain stars spanning a much wider age range. It suggests that the F05 streams are due to an inhomogeneous Galactic potential perturbing smooth star formation rather than the streams resulting from inhomogeneous star formation in a smooth potential. Famaey et al. (2007) show that both situations exist in the N04 sample: the Hyades–Pleiades stream is mainly composed of field-like stars but also partly of coeval stars evaporated from the primordial Hyades cluster (~85 and 15 per cent of the stream for low-mass stars, respectively). Alternatively, Quillen & Minchev (2005) propose the Hyades–Pleiades and Coma Berenices (or local) streams correspond to nearly closed orbits trapped at the 4:1 inner Lindblad resonance of a two-armed spiral density wave.

Dehnen (1998) used a maximum likelihood algorithm to estimate the velocity distribution of the N04 stars before their radial velocities were available using only parallaxes and tangential velocities. He found the traditionally recognized moving groups as well as a smooth background distribution, akin to the Schwarzschild ellipsoidal model, as did F05. The aforementioned streams and the Sirius dynamical stream all share the same region of UV phase space as the Galactic thin disc background (see Fig. 3). The resulting non-Gaussian U and V velocity distributions pose the question: what parametrization of a complex distribution function is adequate to represent a 'dispersion'?

The Gaussianity of the age–σ_W relation permits it to be revisited in this paper. We investigate its derivation from N04 data by checking the stellar warp of the Galactic disc does not contribute to σ_W and that W is sufficiently well mixed that the presence of streams does not cause σ_W of the whole sample to deviate radically from its value for the smooth background (as is certainly happening in σ_U and σ_V). This is demonstrated by showing that dynamical streams do not affect σ_W by deriving the age–σ_W relation with and without the Hercules stream.

The Hercules stream is the only stream in the N04 sample that does not share the same region of UV phase space as the Galactic thin disc background, allowing it to be unambiguously defined in UV phase space and removed in W without also excluding a large region of the background ellipsoid (as would happen in removing one of the other streams). The Hercules stream has been speculated to be a signature of the Galactic bar. Whether Hercules stream stars are chaotically, gravitationally scattered from the inner Galaxy by the Galactic bar (Fux 2001) or they are more local stars coupled to the outer Lindblad resonance (Dehnen 1999, 2000) is still uncertain. Quillen (2003) confirms that the Hercules stream remains a strong feature of the local velocity distribution function when the effect of spiral structure is added to the Galactic bar. Bensby et al. (2007) investigated the abundance and age structure of the Hercules stream. They found that it contains a mixture of young and old stars, all with UV kinematics more characteristic of the thick disc than the thin disc.

Section 2 describes the N04 data used in this paper: survey design (Section 2.1), space velocities (Section 2.2) and discussion on the N04 age derivation (Section 2.3). Our analysis is presented in Section 3, where we reproduce the N04 age–velocity dispersion relation age bins (Section 3.1) and physically interpret them by qualitatively comparing them to the F05 velocity distributions (Sections 3.2 and 3.3). Section 3.4 confirms that the stellar warp of the Galactic disc

does not contribute to σ_W. We revisit the age–σ_W relation using the same age binning as N04 in Section 3.5 and with our own higher resolution age binning in Section 3.6, before discussing our model-fitting results in Section 4.

2 DATA

2.1 Survey design

N04 presented a complete, all-sky, magnitude-limited and kinematically unbiased sample of 16 682 nearby F and G dwarf stars. F and G dwarf stars are good probes of Galactic evolution because they are numerous and long lived. Their radial velocities can be measured accurately and their ages can be estimated by comparison with stellar evolution models, at least for the more evolved stars. Ages are crucial to place the kinematic properties of stars in an evolutionary context. The following section summarizes the properties of N04 most pertinent to revisiting the age–velocity dispersion relation.

The N04 observational input catalogue was selected from a compilation of catalogues available in the literature with Strömgren *uvbyβ* photometry of nearby F and G stars, mainly from the surveys by Olsen (1983, 1993, 1994a,b). The final sample is volume complete to ≈40 pc. It is magnitude complete to $V \leqslant 7.7$ for the bluest stars (slightly fainter for the reddest G stars) and has a V cut-off magnitude of ≈8.9 (and 9.9 for the reddest G stars).

2.2 Space velocities

The input catalogue was observed using the CORrelation RAdial VELocities (CORAVEL) photoelectric cross-correlation spectrometers (Baranne, Mayor & Poncet 1979; Mayor 1985). Two CORAVELs cover the entire sky between them: one is on the Swiss 1-m telescope at Observatoire de Haute-Provence, France, and the other on the Danish 1.5-m telescope at ESO, La Silla. Their fixed, late-type cross-correlation template spectra match the spectra of the majority of the input catalogue stars. The multi-epoch radial velocities (generally two or more spectroscopic observations) have a typical mean error of 0.5 km s^{-1} or less.

The vast majority of the N04 stars have proper motions in the *Tycho-2* catalogue (Høg et al. 2000). This catalogue was constructed by combining the *Tycho* star-mapper measurements of the *Hipparcos* satellite with the Astrographic Catalogue based on measurements in the Carte du Ciel and other ground-based catalogues. A small number of stars have only one measurement, either from *Hipparcos* or *Tycho*. The typical mean error in the total proper motion vector is 1.8 mas yr^{-1}.

The primary source of distance for N04 stars is *Hipparcos* trigonometric parallax (π, ESA 1997), from which absolute magnitude (M_V) can be derived. This is adopted if its relative error (σ_π/π) is accurate to 13 per cent or better, otherwise the photometric distance calibrations for F and G dwarfs by Crawford (1975) and Olsen (1984) are used, with an uncertainty of only 13 per cent. Distances are not provided for stars with unreliable *Hipparcos* parallaxes (>13 per cent) and when photometric distances cannot be calculated. This occurs when the star is missing the necessary photometry and/or it falls outside the photometric calibrations. The absence of a distance estimate or radial velocity measurement reduces the size of the N04 catalogue with all full six-dimensional phase-space information to 13 240 stars. The space velocity components (U, V, W) are computed for all the stars with (mean) radial velocities, proper motions and distances. Space velocities in the VizieR catalogue accompanying N04 are provided to the nearest km s^{-1}. The average error in each component is 1.5 km s^{-1}.

2.3 Ages

2.3.1 N04 age derivation

N04 derive isochrone ages for their stars. Ages are derived by using the photometrically measured effective temperatures (T_{eff}), V magnitudes and metallicity ([Fe/H]) to place stars in the Hertzsprung–Russell diagram and reading off the age of the stars by interpolation between theoretically computed isochrones. T_{eff}, V and [Fe/H] all require extinction correction. The Strömgren β photometry provides interstellar reddening, $E(b - y)$, for F stars via the intrinsic colour calibration by Olsen (1988). This has been applied in the photometric temperature and distance determination if $E(b - y) \geqslant 0.02$ and the distance is above 40 pc, otherwise the stars are assumed to be unreddened. T_{eff} is calculated from the reddening-corrected $b - y, c_1$ and m_1 indices and the calibration of Alonso, Arribas & Martinez-Roger (1996), which is based on the infrared flux method.

The majority of N04 metallicity values are derived using the F or G star calibrations of Schuster & Nissen (1989). Due to the very few spectroscopic calibrators available at the time, the Schuster & Nissen (1989) calibration yields systematic errors for the reddest G and K dwarfs ($b - y > 0.46$). To remedy this, N04 performed a new fit of the *uvby* indices to [Fe/H] derived from high-resolution spectra for 72 dwarfs ($0.44 \leqslant b - y \leqslant 0.59$), using the same terms as the Schuster & Nissen (1989) G star calibration. When valid, N04 adopted the Edvardsson et al. (1993) β and m_1 calibration for stars with high T_{eff} and low gravities outside the Schuster & Nissen (1989) calibrations. For stars outside both calibrations, N04 used other spectroscopic sources to derive a new relation using the same terms as the Schuster & Nissen (1989) F star calibration. The typical [Fe/H] uncertainty is ~0.1 dex.

Individual stellar ages are determined by a Bayesian estimation method. For every point in a dense grid of interpolated Padova isochrones (Girardi et al. 2000; Salasnich et al. 2000) and given a star's nominal position in the three-dimensional Hertzsprung–Russell 'cube' defined by $\log T_{\mathrm{eff}}, M_V$ and [Fe/H], N04 compute the probability that the star is actually located at every point. This procedure takes into account observational errors (Jørgensen & Lindegren 2005). Integrating over all the grid points gives the global likelihood distribution for the possible ages of the star. N04 account for statistical biases in the integration. The resulting probability distribution function ('G-function') is normalized to unity at maximum (see their fig. 13). A stable age estimate without significant bias is given by the maximum of the smoothed G-function. Upper ($\sigma_{\mathrm{age}}^{\mathrm{high}}$) and lower ($\sigma_{\mathrm{age}}^{\mathrm{low}}$) 1$\sigma$ confidence limits are the points where the G-function reaches a value of 0.6.

Isochrone ages can only be determined in practice for stars that have evolved significantly away from the zero-age main-sequence. Therefore, unevolved (i.e. relatively young) stars in the N04 catalogue do not have reliable isochrone ages. This does not affect this study as we are concerned with the functional form of the age–velocity dispersion relation at the evolved end (i.e. old stars) and do not require a complete or unbiased age distribution function.

2.3.2 Age comparisons between N04 and other data sets

Holmberg, Nordström & Andersen (2006) substantially improved temperature and metallicity calibrations of the photometry used by N04, evaluated their effects on the computed ages and performed extensive numerical simulations to verify the robustness of the derived relations. They found good agreement between their new ages and those of N04, supporting the N04 results.

However, Haywood (2002) demonstrates that the original calibration by Schuster & Nissen (1989) is subject to systematic errors, mainly due to incorrect placement of the Hyades reference sequence. Using the same formalism as Schuster & Nissen (1989), Haywood (2002) derived an alternative calibration, which is in good agreement with spectroscopic data sets. Reid et al. (2007) calculated the [Fe/H] difference between Haywood (2002) and N04 and found systematic differences between −0.081 and −0.015 dex for different colour ranges. Reid et al. (2007) also compared the photometrically derived [Fe/H] of N04 and Haywood (2002) with high-resolution echelle spectroscopically derived [Fe/H] obtained by the Keck, Lick and AAT planet search programs (Valenti & Fischer 2005). They found that while the dispersions were similar (∼0.1 dex), the difference between Valenti & Fischer (2005) and Haywood (2002) (−0.041 to +0.045 dex) is smaller than between Valenti & Fischer (2005) and N04 (0.015–0.090 dex).

Since the N04 ages are derived from isochrone fitting, systematic [Fe/H] errors translate to systematic age offsets. As a recalculation of the N04 ages to investigate the effect of systematic [Fe/H] errors is unnecessary for this paper, we proceed with the assumption that any age offset will have a negligible impact on our statistical use of age in this study. In addition, we are only using single stars with well-defined ages and age errors, so we assume the N04 age errors are the appropriate errors.

3 ANALYSIS

### 3.1 Reproducing the N04 age–velocity dispersion relation age bins

N04 caution that many stars in their sample are binary or multiple systems, for which the derived metallicities and thus ages will be unreliable. They provide a catalogue flag (f_b) that identifies confirmed or suspected binaries, where the information can come from one or several sources such as photometry, radial velocity or astrometry. N04 used only single stars (as defined by a null f_b catalogue entry, 8589 stars) with relative age errors <25 per cent (2852 stars) to derive their age–velocity dispersion relations in their fig. 31. Our attempt to reproduce this sample by rejecting stars with f_b catalogue entries to define single stars and selecting stars with (σ_{age}^{high} − age)/age ⩽ 0.25 and (age − σ_{age}^{low})/age ⩽ 0.25 yields a smaller sample (2801 stars). The missing 51 stars are presumably due to N04 using more precise ages than their catalogue ages, which have been rounded up to the nearest 0.1 Gyr.

N04 split their sample of single stars with relative age errors <25 per cent into 10 age bins of equal numbers. Due to the presumably lower age resolution in their catalogue, we are unable to make the numbers of stars in each of our age bins exactly the same. This means that the boundaries of our age bins are only similar to those used by N04, rather than being exactly the same. Unlike N04, we plot the space velocity diagrams (Fig. 1) and histograms (Fig. 2) of a representative age bin (plots of all the age bins are in Appendix A). The 3 km s^{-1} velocity bin sizes in Fig. 2 (and Fig. A2) are chosen to be twice the average error in each component of the N04 space velocities so that substructure can be resolved (F05 found the Hyades–Pleiades and Sirius dynamical streams have $\sigma_V \approx 5$ km s^{-1}). From the apparent lack of substructure in Fig. 1 (and Fig. A1), it is not clear in Fig. 2 (and Fig. A2) whether the peaks in the histograms are Poisson noise, due to the relatively small number of stars in each bin at this velocity resolution, or substructure. Decomposition of the N04 sample into its constituent kinematic groups, like F05, is beyond the scope of this paper. Instead, we qualitatively compare the N04 and F05 space velocity diagrams and histograms to assess whether we expect complex substructure in all the age bins in Figs A1 and A2 or whether the peaks are noise such that the distribution functions can be approximately described by Gaussians.
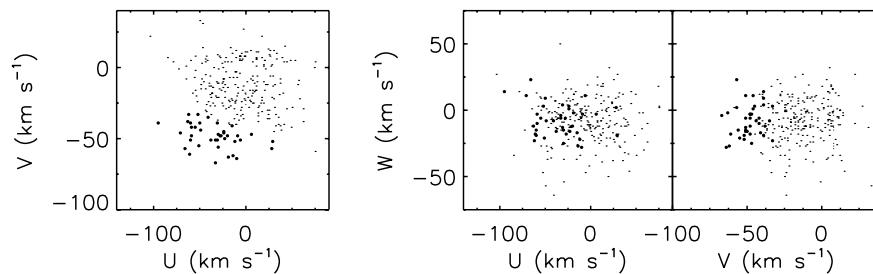
Figure 1. $U-V$ (left-hand panel), $U-W$ (middle panel) and $V-W$ (right-hand panel) space velocity diagrams of the 278 N04 single stars with relative age errors <25 per cent in the 2.8 < age ⩽ 4.6 Gyr age bin. We have assigned 39 N04 stars in this age bin to the Hercules stream (filled circles) using the Hercules stream UV phase space (defined by F05, see Fig. 3) and the Hercules stream W phase space (defined by F05, see Figs 4 and 5).
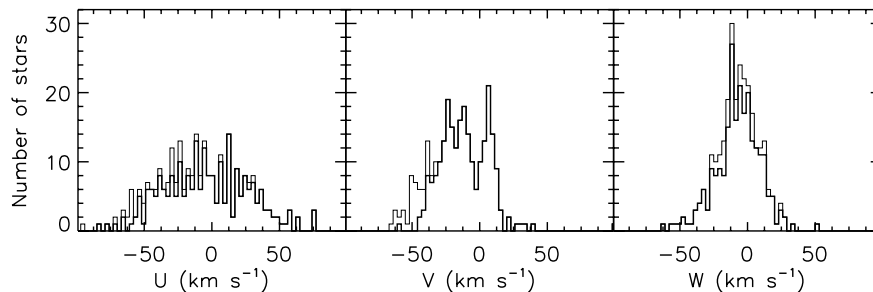
Figure 2. U (left-hand panel), V (middle panel) and W (right-hand panel) velocity distributions of the N04 single stars with relative age errors <25 per cent in the 2.8 < age ⩽ 4.6 Gyr age bin (thin line) and a subsample of these stars that excludes the Hercules stream (thick line), as defined in Figs 3–5.

## 3.2 Comparison of N04 and F05 kinematic analysis

F05 also published a VizieR catalogue accompanying their paper, based on the CORAVEL radial velocities of 6691 Northern hemisphere stars. Unfortunately, unlike the N04 stars, the F05 stars do not have individual stellar ages so F05 cannot be used to revisit the age–velocity dispersion relation of the smooth background and investigate the effects of each dynamical stream on the relation. Instead in this section, we describe how F05 decomposed their sample into its constituent kinematic components and compare their phase-space substructure with N04 in order to physically motivate our assessment of Figs 1 and 2 (and Figs A1 and A2).

The basic technique to calculate space velocities is to invert the parallax to estimate the distance. This is then used to compute the tangential space motion components from the proper motions, which in combination with radial velocities can be transformed to the Galactocentric frame. Due to the non-linearity of the parallax–distance transformation, if σ_π/π is high, the inverse parallax is a biased estimator of the distance and an individual error on a space velocity cannot be derived from a simple first-order linear propagation of σ_π. As all the stars in N04 are relatively nearby, most have parallaxes with σ_π/π better than 10 per cent and nearly all are better than 20 per cent. The availability of photometric distances with an uncertainty of only 13 per cent means the parallax inversion derived distances adopted for N04 stars when $\sigma_\pi/\pi < 13$ per cent only have a very small distance bias (Brown et al. 1997), which does not affect the calculation of space velocity errors.

The resulting space velocity diagrams, restricted to the 8589 single N04 stars, are plotted in the left-hand columns of Figs 3–5 (cf. N04's fig. 20 of the whole sample). While the *U–W* (Fig. 4) and *V–W* (Fig. 5) diagrams show a smooth distribution, the *U–V* diagram (Fig. 3) shows abundant phase-space substructure. It consists of four tilted branches aligned along approximately constant *V* velocities that resemble classic moving groups or stellar streams named, from top to bottom, the Sirius-UMa, Coma Berenices (or local), Hyades–Pleiades and ζ Herculis branches. These branches are only loosely defined as overdensities in phase space. N04's straightforward space velocity derivation does not include assignment of individual stars to these branches, only its position in phase space.
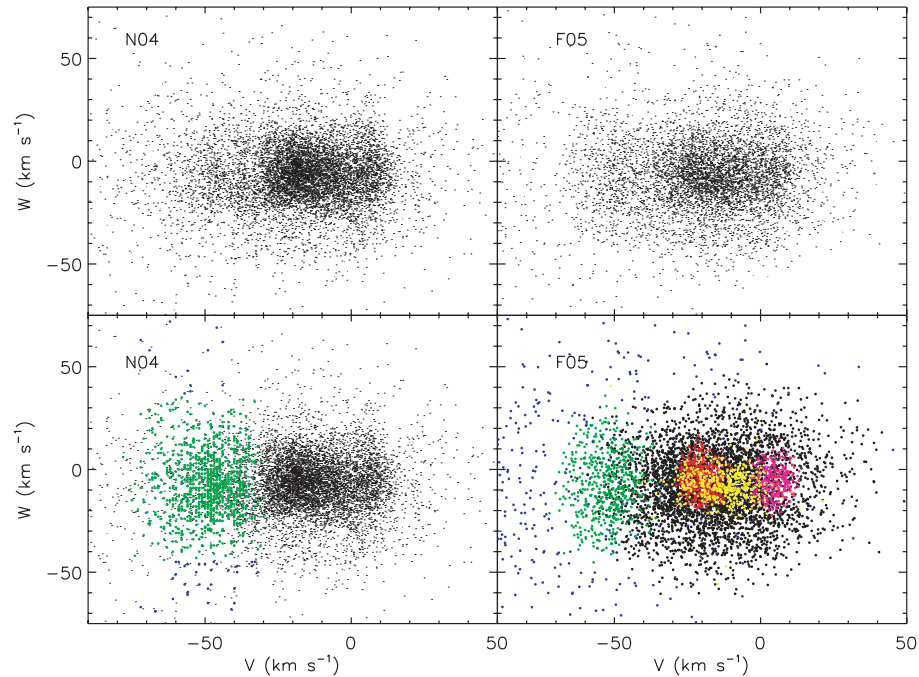
F05 binaries for which no centre-of-mass radial velocity could be estimated were removed from their sample using their binarity flag (*B*). A star was excluded in their kinematic analysis if it was a spectroscopic binary (*B* = 0) or a visual binary with no orbit available (*B* = 5) or an uncertain case, either a spectroscopic binary or supergiant (*B* = 3) or for a visual binary (*B* = 8), leaving 6030 stars (5311 K and 719 M giants). Because the F05 giants are at distances approximately an order of magnitude greater than the N04 dwarfs, the F05 distribution of σ_π/π is correspondingly less accurate than that of N04. There are only 786 F05 stars with $\sigma_\pi/\pi < 10$ per cent, which is too small a sample to characterize the K and M giants in the solar neighbourhood. $\sigma_\pi/\pi < 20$ per cent increases the sample size to 2774 stars (2524 K and 250 M giants). With this accuracy, the distance bias is still very small and the first-order approximation for the calculation of space velocity errors is still valid. The resulting density of stars in the *U–V* diagram with $\sigma_\pi/\pi < 20$ per cent reveals overdensities in the same region of phase space as the N04 branches (see F05's fig. 7). We therefore consider that the F05 kinematic phase-space structure seen at distances of a few hundred pc is consistent with that seen locally by N04.
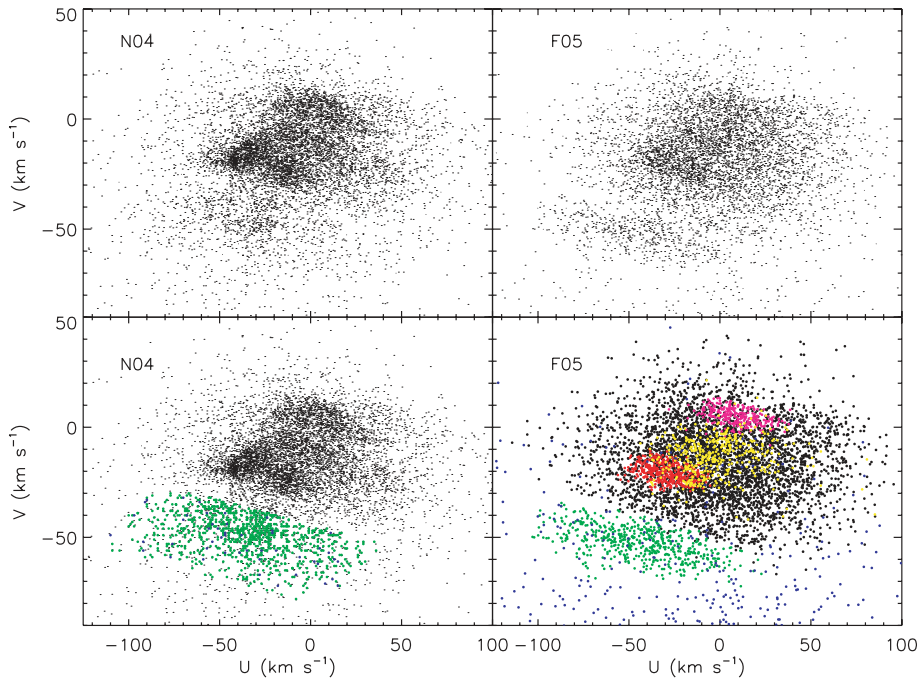
Figure 3. *U–V* diagrams of the 8589 N04 single F–G dwarfs with space velocities (left-hand column) and the 6030 F05 K–M giants with space velocities, including spectroscopic binaries with centre-of-mass radial velocities (right-hand column). The overdensity at $(U, V) = (-45, -20)$ km s^{-1} in the left-hand column is the Hyades open cluster (only in the N04 sample). In the bottom left-hand panel, the N04 stars are colour-coded according to our assignment of N04 stars to the Hercules stream (green) and high-velocity stars (blue) in the Hercules stream *UV* phase space (defined by F05, bottom right-hand panel) but outside the Hercules stream *W* phase space (see Figs 4 and 5). In the bottom right-hand panel, the F05 stars are colour-coded according to their maximum likelihood base group assignment to known kinematic features of the solar neighbourhood: smooth background (black), Sirius moving group (magenta), young kinematics (yellow), Hyades–Pleiades supercluster (red), Hercules stream (green) and high-velocity stars (blue).
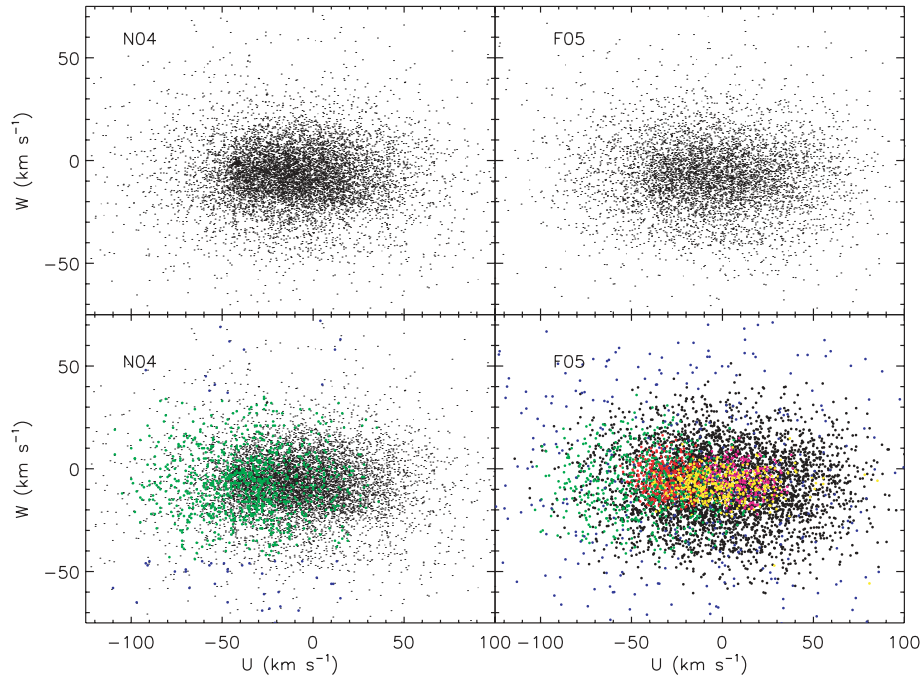
Figure 4. *U–W* diagrams of the 8589 N04 single F–G dwarfs with space velocities (left-hand column) and the 6030 F05 K–M giants with space velocities, including spectroscopic binaries with centre-of-mass radial velocities (right-hand column). The overdensity at $(U, W) = (-45, 0)$ km s^{-1} in the left-hand column is the Hyades open cluster (only in the N04 sample). In the bottom left-hand panel, the N04 stars are colour-coded according to our assignment of N04 stars to the Hercules stream (green) and high-velocity stars (blue) in the Hercules stream *UV* phase space (defined by F05, see Fig. 3) but outside the Hercules stream *W* phase space (defined by F05, bottom right-hand panel). In the bottom right-hand panel, the F05 stars are colour-coded according to their maximum likelihood base group assignment to known kinematic features of the solar neighbourhood: smooth background (black), Sirius moving group (magenta), young kinematics (yellow), Hyades–Pleiades supercluster (red), Hercules stream (green) and high-velocity stars (blue).

Figure 5. *V–W* diagrams of the 8589 N04 single F–G dwarfs with space velocities (left-hand column) and the 6030 F05 K–M giants with space velocities, including spectroscopic binaries with centre-of-mass radial velocities (right-hand column). The overdensity at $(V, W) = (-20, 0)$ km s^{-1} in the left-hand column is the Hyades open cluster (only in the N04 sample). In the bottom left-hand panel, the N04 stars are colour-coded according to our assignment of N04 stars to the Hercules stream (green) and high-velocity stars (blue) in the Hercules stream *UV* phase space (defined by F05, see Fig. 3) but outside the Hercules stream *W* phase space (defined by F05, bottom right-hand panel). In the bottom right-hand panel, the F05 stars are colour-coded according to their maximum likelihood base group assignment to known kinematic features of the solar neighbourhood: smooth background (black), Sirius moving group (magenta), young kinematics (yellow), Hyades–Pleiades supercluster (red), Hercules stream (green) and high-velocity stars (blue).

To make full use of all their 6030 stars and to assign individual stars to each phase-space branch in order to investigate their kinematics, F05 applied the Luri–Mennessier method to their data. This maximum likelihood method is based on a Bayesian approach and is described in detail in Luri et al. (1996). It requires a model describing the basic morphological characteristics of the sample (spatial distribution, kinematics and M_V) and a model of the selection criteria used to define the sample. A total distribution function is built using these models to describe the observational characteristics of the sample. This consists of a linear combination of partial distribution functions, each of which describes a group of stars called a 'base group'. Each of these combines a velocity ellipsoid with a Gaussian magnitude distribution and exponential height distribution perpendicular to the Galactic plane. The advantage of this phenomenological model is that it can identify and quantify different subgroups in the data, which cannot be easily parametrized using other methods. A maximum likelihood fit of the model parameters to the sample yield the model parameters that best represent the sample given the a priori models assumed.

The expected space velocities deduced by the Luri–Mennessier method of the 6030 F05 stars are plotted in the right-hand columns of Figs 3–5 (cf. F05's fig. 9). Modelling this sample with a single base group returns a low maximum likelihood, suggesting to F05 that a single Schwarzschild ellipsoid does not fit the kinematic properties of giant stars in the solar neighbourhood. The first acceptable solution they found required three base groups: bright giants/supergiants with 'young' kinematics, high-velocity stars and 'normal' stars. This last group contained further small-scale structure, which F05 successfully modelled by three more statistically significant base groups. Although adding more groups produced statistically better solutions, F05 found that these solutions were not stable because they depended too much on the observed values of some individual stars. F05 identified the resulting six base groups with known kinematic features in the solar neighbourhood (colour-coded in the bottom right-hand panels of Figs 3–5), which are also seen in the N04 phase space.

Despite all the differences described above, Figs 3–5 show the N04 and F05 phase space is remarkably similar, suggesting the F05 kinematic base group assignment describes structures covering several hundred pc in the solar neighbourhood at least to first order, again suggesting the structures are not remnants of single small star clusters. We therefore consider the N04 branches to have the same physical origin as postulated by F05 for their corresponding base groups.

3.3 Comparison of N04 and F05 phase space

We compare the space velocity distributions of the N04 and F05 stars in Fig. 6. This highlights the departures from Gaussianity of the U and V distribution functions caused by the presence of streams compared to W, which approximates a Gaussian, due to the tilt of these streams in the UV plane in Fig. 3, measured to be $V =$ constant $-0.47U$ by Skuljan, Hearnshaw & Cottrell (1999). A direct comparison between the N04 and F05 distributions is interesting because Figs 3–5 show that the N04 substructures are more prominent than the F05 substructures compared to their smooth backgrounds apparently due to the difference in scaleheight between the two samples, illustrated in Fig. 7. The much lower scaleheight of the N04 sample and its more prominent substructure means dynamical streams are more prominent in stars close to the plane due to a mix of dynamics and sample age differences.

Another difference is that there are similar numbers of stars in each of the F05 streams but the N04 V distribution in Fig. 6 shows that this is not the case in the N04 sample as it is more numerically dominated by the much narrower peak of the Hyades–Pleiades stream at $V \sim -20$ km s^{-1} than in the F05 V distribution. This is because the N04 completeness out to $\sim$40 pc includes the Hyades cluster itself (visible in Figs 3–5). Famaey et al. (2007) showed
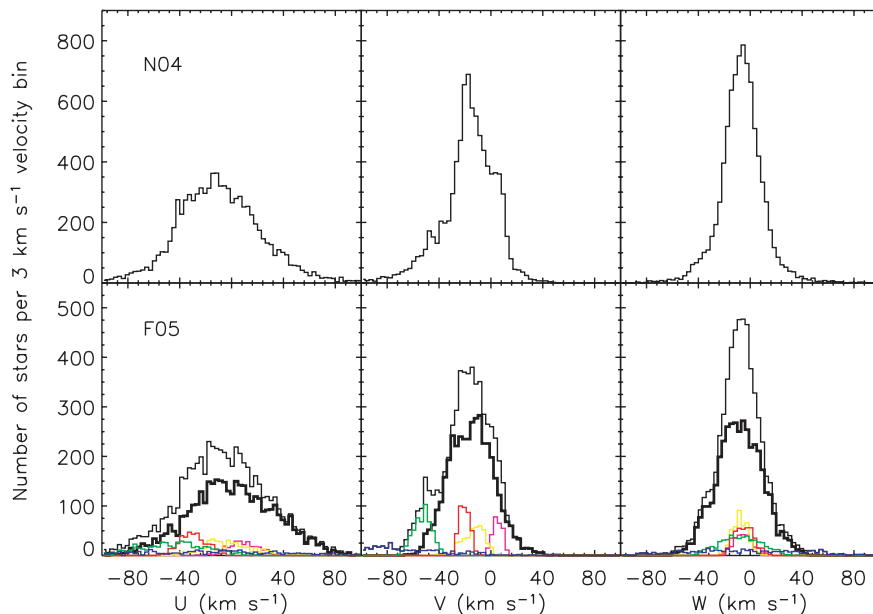
Figure 6. U (left-hand panels), V (middle panels) and W (right-hand panels) velocity distributions of the 8589 N04 single F–G dwarf stars with space velocities (top row, thin black lines) and the 6030 F05 K–M giants with space velocities (bottom row, thin black lines), including spectroscopic binaries with centre-of-mass radial velocities, colour-coded according to their maximum likelihood base group assignment to known kinematic features of the solar neighbourhood: smooth background (thick black lines), Sirius moving group (magenta), young kinematics (yellow), Hyades–Pleiades supercluster (red), Hercules stream (green) and high-velocity stars (blue).
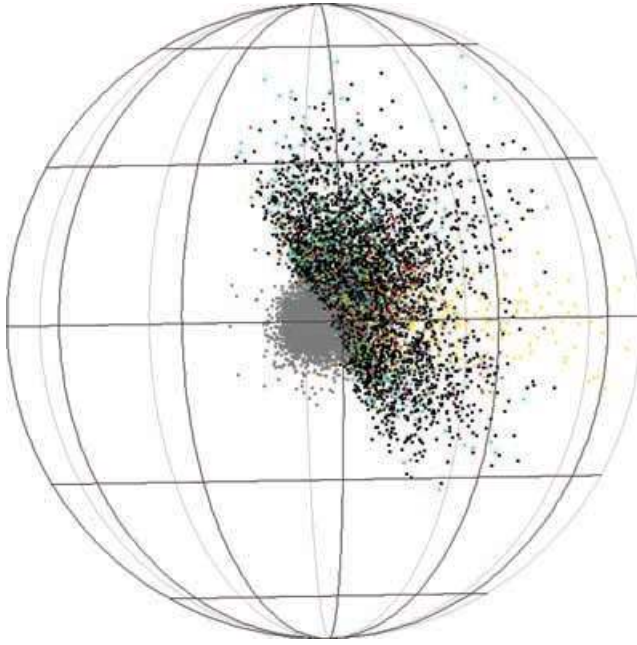
Figure 7. Three-dimensional Galactic sky distribution of the 8589 N04 single F–G dwarfs with space velocities (grey) and the 6030 F05 K–M giants with space velocities, including spectroscopic binaries with centre-of-mass radial velocities, colour-coded according to their maximum likelihood base group assignment to known kinematic features of the solar neighbourhood: smooth background (black), Sirius moving group (magenta), young kinematics (yellow), Hyades–Pleiades supercluster (red), Hercules stream (green) and high-velocity stars (blue). The spherical polar axes have a radius of 900 pc, centred on the Sun. The viewer is in the Galactic plane, inside the solar circle at $l = 30°$ (the Galactic Centre is over the viewer's left-hand shoulder). The viewer's angle has been chosen to illustrate the 63° between the Earth's equator and the Galactic plane (longest horizontal line), emphasizing that the F05 sample only contains stars visible from the Earth's Northern hemisphere. The nearest line of constant Galactic longitude is $l = 30°$ (with the majority of the stars behind it). l increases to the right-hand side (anticlockwise) with lines of constant Galactic longitude every 30°. All the lines of constant Galactic longitude converge at the North Galactic Pole ($b = +90°$, top) and at the South Galactic Pole ($b = −90°$, bottom), with lines of constant Galactic latitude every 30°.

Table 1. Comparison of N04 and F05 velocity dispersions (in km s^{-1}) of combinations of different F05 kinematic groups: smooth background (B), Sirius moving group (S), young kinematics (Y), Hyades–Pleiades supercluster (HyPl), Hercules stream (He) and high-velocity stars. (Each dispersion is an outlier-resistant measure of the dispersion about the centre of the velocity distribution calculated by using the median absolute deviation as the initial estimate, then each star is weighted using Tukey's biweight. For a Gaussian distribution, this is identical to the standard deviation.)

Dispersion	σ_U	σ_V	σ_W
N04 all	32.6 ± 0.2	20.0 ± 0.2	15.1 ± 0.1
B	33.8 ± 0.4	17.4 ± 0.2	17.8 ± 0.2
Si, Y, HyPl	22.3 ± 0.5	12.2 ± 0.3	7.0 ± 0.2
B, Si, Y, HyPl	31.8 ± 0.3	16.4 ± 0.2	15.7 ± 0.2
B, Si, Y, HyPl, He	33.7 ± 0.3	19.6 ± 0.2	15.8 ± 0.1
F05 all	35.6 ± 0.3	22.0 ± 0.2	17.1 ± 0.2

and A2 are in fact dynamical streams rather than noise. We can also use Fig. 6 to interpret the N04 U and W distributions. It suggests that many of the minor peaks in these distributions are noise. However, like in V, the F05 streams do not share similar mean U velocities so the N04 U distribution is also complex and non-Gaussian. We conclude that N04's treatment of the U and V distributions with a straightforward dispersion was an inadequate parametrization of these complex distribution functions. The interpretation of an age–velocity dispersion relation for U and V is non-trivial and beyond the scope of this paper.

Nevertheless, these complex distribution functions raise the interesting issue as to what constitutes disc heating. In Section 1, we defined it as processes that change stellar velocities in any direction such that the velocity dispersion increases. If this heating is random in direction it will fill and shape the velocity ellipsoid slowly over time. However, if processes like those responsible for dynamical streams (transient spiral waves and/or resonances) overpopulate a specific subregion of phase space, then the concentration of these stars relative to the background can actually change the overall components of the velocity dispersion by weighting them to the mean velocities of the streams. This scenario is illustrated in Table 1. It reveals that the F05 background dispersions are systematically slightly larger than the dispersions of the background and thin disc streams combined. This shows that the F05 streams decrease the dispersions of the background and thin disc streams combined by weighting them to the mean velocities of the streams so that the combined dispersion differs slightly from the background dispersion. Therefore, the mechanism responsible for the F05 thin disc streams could be considered a disc 'cooling' agent. The inclusion of the Hercules stream and high-velocity stars increases the overall dispersion to greater than the background alone so they could be considered as 'heating' agents. However, this classification is specific to the F05 sample. The dominance of the N04 streams over the N04 background complicates the U and V distributions more than in F05. The differing strengths with stellar age of the streams, makes it difficult to estimate whether the overall σ_U and σ_V will be heated or cooled by the presence of streams compared to the background as a function of time, without prior knowledge of the properties of the N04 background, which are non-trivial to derive given the dominance of the streams. Therefore, we are unable to generalize which specific mechanisms constitute disc heating or cooling because it depends on the sample considered.

N04 excluded the youngest age bin from their power-law fit to avoid biases due to unrelaxed young structures. The non-Gaussianity

that, in addition to bound Hyades cluster stars, the Hyades–Pleiades stream is mainly composed of field-like stars but also partly of coeval stars evaporated from the Hyades cluster. F05 actually propose that because the cluster is young (600 Myr), it should not have crossed many spiral structures, suggesting that the same transient spiral wave that formed it (by boosting star formation in its primordial gas cloud) could at the same time have given it and nearby field stars their peculiar velocity in the *UV* plane. For any evaporated cluster stars to get into the much higher scaleheight of the F05 sample requires them to have experienced phase-mixing and vertical disc heating. They are more likely to have had their initial birth velocities erased and so are less likely to be identifiable as evaporated cluster stars in the F05 sample.

F05 showed that their dynamical streams span several Gyr in age, which is supported theoretically by the simulations of De Simone et al. (2004). Therefore, we expect the F05 streams in Fig. 6 to be present in the N04 sample over many age bins as narrow peaks in the V histograms in Figs 2 and A2, which allows us to trace the changing relative strengths of these streams with stellar age. This suggests that the majority of the peaks in the V histograms in Figs 2

of some of the *W* histograms of the young thin disc (0.5 < age ⩽ 2.8 Gyr) bins (see Fig. A2) suggests that the N04 sample does not vertically relax until the stars are older than this age range. The *W* histograms of the 2.8 < age ⩽ 4.6 Gyr (see Fig. 2) and 4.6 < age ⩽ 7.6 Gyr bins (see Fig. A2), representing the old thin disc, are more Gaussian and thus can be considered relaxed. We conclude that N04's treatment of the *W* distribution with a straightforward dispersion may not be an adequate parametrization of the young thin disc but it is adequate for the old thin disc. This does not affect their general result because σ_W must increase with time in order for the older thin disc to have a higher scaleheight than the young thin disc. It does not affect our aims here because we are only concerned with the functional form of the relation for the old thin disc.

It has long been known that traditional moving groups are indistinguishable in the vertical direction because the *W* velocity distribution function appears to be well phase-mixed (Dehnen 1998). This is theoretically expected as phase-mixing of vertical space motions is more efficient than for the horizontal space motions because, for a realistic disc profile, the vertical frequency is a strong function of vertical energy and the vertical dynamical time is a factor of 2 shorter than the horizontal orbital period. Consequently, *W* motion is decoupled from *U* and *V* motions, suggesting that dynamical streams should not affect a star's *W* velocity. Table 2 in F05 suggest that all the streams share similar mean *W* (⟨*W*⟩). We test this in the following section.

3.4 Stellar warp of the Galactic disc

Dehnen (1998) found that his outermost contours of phase-space density are skewed relative to the *W* axis in the sense that more stars moving faster than the local standard of rest (LSR, +*V*) are

Table 2. χ^2 goodness-of-fit test results between the data and model in Fig. 8. *n* is the number of data points included in the model fit. n_c is the number of constraints on each model fit (only one to normalize each model to each data set). The number of degrees of freedom is $\nu = n - n_c$. The χ^2 probability distribution function for ν degrees of freedom, $Q(\chi^2 \mid \nu)$, is the standard statistical significance of the χ^2 test $[Q(\chi^2 \mid \nu) = 1 - P(\chi^2 \mid \nu)]$.

Sample	n	n_c	ν	χ^2	χ^2/ν	$Q(\chi^2 \mid \nu)$
N04 *V* > 15	13	1	12	19.0	1.58	0.089
F05 *V* > 15	11	1	10	16.5	1.65	0.087
N04 all *l*	36	1	35	45.2	1.29	0.117
F05 all *l*	36	1	35	47.1	1.35	0.083

also moving upward with respect to the LSR (+*W*) than downwards (−*W*). His fig. 6 shows that ⟨*W*⟩ is approximately constant at the W_{LSR} value for $V \lesssim 10$ km s^{-1} but curves upward for $V \gtrsim 10$ km s^{-1}. He interprets this curve as the signature of a stellar warp in the Galactic disc, which starts at the solar circle. If there are lots of N04 stars in the warp and these stars are included in our analysis, the departure from a constant ⟨*W*⟩ would artificially increase σ_W. This would bias the true σ_W so that it could appear as though there is more disc heating than in the assumed flat disc case (approximately constant W_{LSR} with respect to *V*).

To check whether this source of σ_W bias is present in the N04 data set, we reproduce fig. 6 from Dehnen (1998) for the N04 and F05 samples in the left-hand column of Fig. 8. Contrary to his claim, we do not find a signature of a stellar warp in the Galactic disc in either data set. Fig. 3 shows that the number of stars decreases with +*V* in both data sets, which is reflected in the large error bars in Fig. 8 at high values of +*V*.
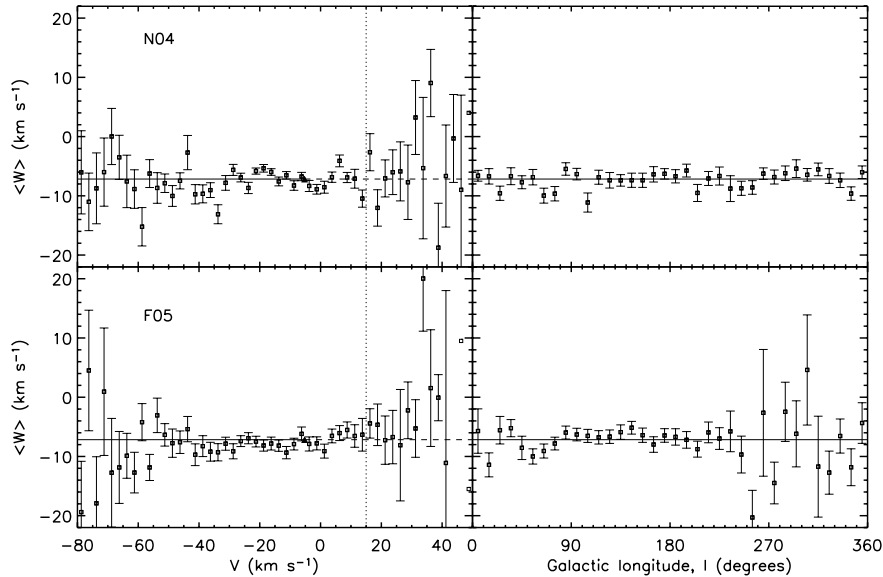
Figure 8. Robust mean vertical motion (⟨*W*⟩) as a function of *V* (left-hand column, same *V* plot range, velocity bin centres and 2.5 km s^{-1} velocity bin widths as fig. 6 in Dehnen 1998) and as a function of Galactic longitude, *l* (right-hand column) for the N04 single F–G dwarfs and the F05 K–M giants. 8386 N04 stars are included in the top left-hand plot out of a possible 8589 (98 per cent), whereas all are included in the top right-hand plot. 5852 F05 stars are included in the bottom left-hand plot out of a possible 6030 (97 per cent), whereas all are included in the bottom right-hand plot. The triangle indicates the velocity of the LSR with respect to the Sun: $(V_{LSR}, W_{LSR}) = (-V_{\odot}, -W_{\odot}) = (-5.25, -7.17)$ km s^{-1} (Dehnen & Binney 1998). The horizontal solid lines along W_{LSR} out to the LSR represents a flat Galactic disc out to the solar circle. The horizontal dashed lines outwards from the LSR represent a model of the flat disc continuing outside the solar circle instead of a stellar warp in the disc, as proposed by Dehnen (1998). The χ^2 tests compare the data to the model to the right-hand side of the vertical dotted lines at *V* = 15 km s^{-1} (set to exclude the maximum *V* bins containing Sirius dynamical stream stars). Data points without error bars on ⟨*W*⟩ only contain one star and are thus excluded from the χ^2 tests (as is the empty F05 bin 42.5 < *V* ⩽ 45.0 km s^{-1}).

The N04 sample in the top left-hand panel of Fig. 8 is averaged over the entire sky. H I observations show that the Galactic disc is flat out to approximately the solar circle and then the warp turns up towards the North Galactic Pole in the $l \sim 90°$ direction, while turning towards the South Galactic Pole in the $l \sim 270°$ direction. If the N04 and F05 stars share the gas kinematics of the warp, then their participation in the warp would be seen by $\langle W \rangle > 0$ towards $l \sim 90°$ and $\langle W \rangle < 0$ towards $l \sim 270°$. It is conceivable that if the warp is symmetric in amplitude about the plane and symmetric in l, then its signature could cancel itself out and result in a flat $\langle W \rangle$ as a function of V in the top left-hand panel of Fig. 8. Plotting $\langle W \rangle$ as a function of l in the right-hand column of Fig. 8 confirms this is not the case and that there is no sinusoidal signature of the warp in l. The F05 sample becomes noisy at $l > 230°$ because of incomplete coverage of the Galactic sky (see Fig. 7 and F05 fig. 6).

Table 2 shows that $Q(\chi^2 \,|\, \nu) > 0.003$ [$P(\chi^2 \,|\, \nu) < 0.997$] for all the tests so both data sets accept the flat disc model at the 3σ statistical significance level. However, the model is not strongly accepted as would be indicated by high $Q(\chi^2 \,|\, \nu)$ values. This is because for each data set, there is one V bin at similar V values (32.5 < $V \leqslant$ 35.0 and 35.0 < $V \leqslant$ 37.5 km s^{-1} for F05 and N04, respectively) for which the $\langle W \rangle$ is more than $2\Delta\langle W \rangle$ away from the flat disc model of constant W_{LSR} (i.e. no warp). It is these bins that cause the low $Q(\chi^2 \,|\, \nu)$ values in Table 2. Respectively, the six and four stars in these bins do not share similar W velocities as would be expected if they were part of a warp or stream. These bins have very wide ranges of W velocities, perhaps because one or more of these stars are members of the thick disc or halo. The small number of stars in each bin results in the data points being offset from the rest.

Therefore, contrary to Dehnen (1998), we do not find a signature of the stellar warp in the Galactic disc in the N04 or F05 samples. This means that the N04 sample has an approximately constant $\langle W \rangle$. The small ($\sim$2 km s^{-1}) excursions from W_{LSR} as a function of V do coincide with the V values of the streams in the N04 sample. These small net vertical motions are presumably due to the young unrelaxed stars evaporating from star clusters rather than field stars caught in the dynamical streams.

The lower scaleheight of the N04 sample in Fig. 7 means its smooth background σ_W will be less than the F05 background σ_W in Table 2. Famaey et al. (2007) showed that $\sim$15 per cent of the N04 Hyades–Pleiades stream is evaporated coeval Hyades cluster stars. Assuming an initial velocity dispersion $\sigma_0 \sim 10$ km s^{-1}, the evaporated Hyades stars will manifest themselves as a clump in the velocity distribution function that is narrow in V (because all the stars have identical angular momentum) but has size $\gtrsim \sigma_0$ in U and W (Woolley 1961). Therefore, the N04 Hyades–Pleiades stream should have a larger σ_W than the purely dynamical F05 Hyades–Pleiades stream (this may also be the case for the other streams). Hence, the N04 background σ_W is likely to be more similar to the N04 thin disc streams σ_W than in the F05 case. Thus the overall N04 W distribution is a sum of similar σ_W and similar $\langle W \rangle$ Gaussians, which is a Gaussian with similar σ_W and similar $\langle W \rangle$. Having established that the only component of the age–velocity dispersion relation that can be simply measured locally is the vertical component, the rest of the paper concentrates on revisiting N04's age–σ_W relation.

3.5 Reproducing the N04 age–σ_W relation

Fig. 6 shows that the Hercules stream has a larger σ_W than the other F05 streams. This may be due to its different dynamical origin from the other streams: perhaps the Galactic bar. Bensby et al. (2007) showed that the Hercules stream includes both younger and old disc

stars and they suggest some thick disc stars may be included. The Hercules stream σ_W may be larger due to the thick disc stars in the stream retaining their characteristically higher σ_W, which is a property of the thick disc. Alternatively, the higher σ_W may be a dynamical signature of the bar, imparted to both its constituent thin and thick disc stars as they interacted with the bar. If it is the latter and the N04 Hercules stream σ_W is sufficiently different from the N04 smooth background and thin disc streams, then the thin disc Hercules stream stars could bias the age–σ_W relation. The smooth W distributions in Figs 4 and 5 suggest σ_W is a valid description of the W distribution function, unbiased by kinematic substructure because the W distribution is well phase-mixed. By deriving the age–σ_W relation both with and without the Hercules stream, we can simultaneously test whether the relation is biased by the stream and whether the W distribution is well phase-mixed, implying the presence of the thin disc streams does not affect the relation.

We use the most extreme F05 Hercules stream stars in U and V to define the N04 Hercules stream UV region in Fig. 3. Figs 4 and 5 are also used to identify high-velocity stars within the UV region of the Hercules stream that have W velocities that are outside the Hercules stream W region and thus are more likely to be part of the thick disc velocity ellipsoid. This technique will only identify high-velocity stars with more extreme thick disc or halo kinematics. Therefore, the removal of Hercules stream stars will also remove some high-velocity stars but this is of no consequence to our study. These stars are colour-coded in Figs 3–5. Every figure from here onwards both includes and excludes Hercules stream stars.

Fig. 9 shows that a robust (bisquare-weighted) mean age of an age bin is sometimes quite different from the central age of that bin. By comparison with N04's fig. 31, we find that we are best able to reproduce their age–σ_W relation using both robust ages and robust dispersions in Fig. 10. The error bars in Fig. 10 are the errors in calculating a standard deviation:

$$\Delta\sigma_W = \frac{\sigma_W}{\sqrt{2N}}, \tag{1}$$

where N is the number of stars in each age bin used to calculate σ_W. The logarithmic spacing of the age bins in Fig. 10 is a natural consequence of N04's decision to have equal numbers of stars in each of their age bins because the distribution of stellar ages is logarithmic. This also naturally leads N04 (and us) to fit a power law:

$$\sigma_W = a\,\text{age}^k, \tag{2}$$

where a is a constant and k is the scaling (heating) exponent. Taking the log of both sides of equation (2) gives

$$\log_{10}(\sigma_W) = k\log_{10}(\text{age}) + \log_{10}(a), \tag{3}$$

which produces a linear relationship where k is now the slope and $\log_{10}(a)$ is the intercept. A linear least-squares fit gives $k = 0.48 \pm 0.26$ (including the Hercules stream, $k = 0.50 \pm 0.25$ excluding Hercules stream), which is similar to N04's $k = 0.47 \pm 0.05$. However, we can only reproduce their quoted uncertainty by excluding errors from the fit: $k = 0.45 \pm 0.04$. We are thus able to reproduce and verify the N04 age–σ_W relation using the rounded up catalogue data.

These values of k are close to the $k = 0.50$ predicted by Hänninen & Flynn (2002) for vertical disc heating by halo black holes of mass 1×10^7 M$_\odot$. The goodness of fit of these power laws are therefore a test of how well the data are represented by this source of heating. Hänninen & Flynn (2002) also predict $k = 0.26$ for the vertical heating exponent by GMCs, where the constant a in equation (2)
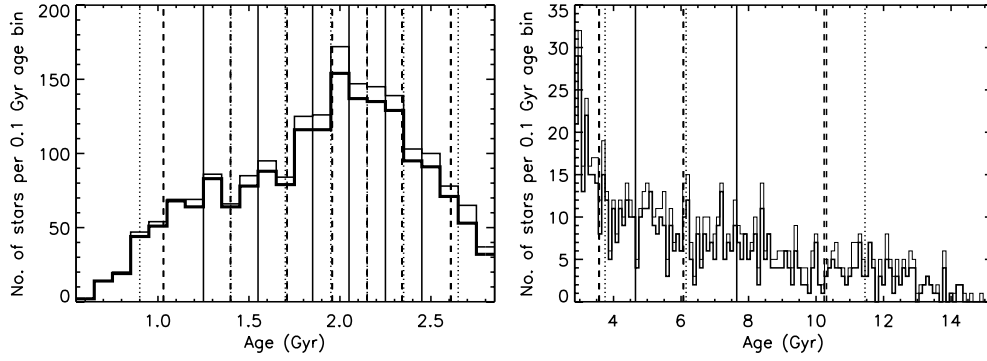
Figure 9. Discrete age distribution of the N04 single stars with relative age errors < 25 per cent, split between the youngest seven age bins from Fig. A2 (left-hand panels) and the oldest three age bins from Fig. A2 (right-hand panels). The thin lines correspond to the whole sample and the thick lines are the subsample excluding the Hercules stream. Because the N04 catalogue stellar ages are provided to the nearest 0.1 Gyr, each 0.1-Gyr histogram bin only contains stars with the exact age that its histogram step is centred on, for example, the youngest histogram bin, centred on 0.6 Gyr, only contains stars with exactly 0.6 Gyr ages but the histogram step spans 0.55–0.65 Gyr. The vertical solid lines (including the vertical edges of the plots) are the boundaries to the age bins. The dotted lines are the central ages of each age bin. The robust mean ages within each age bin for the whole sample (thin-dashed lines) and subsample (thick-dashed lines) are indistinguishable apart from the oldest age bin.
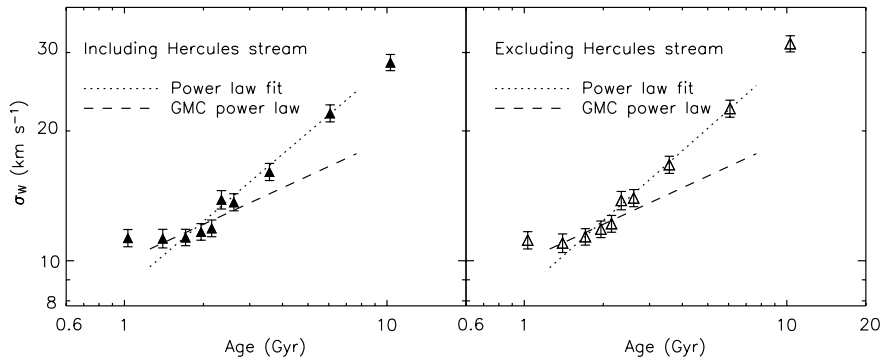
Figure 10. N04 logarithmic age–σ_W relation: robust σ_W of N04 single stars with relative age errors <25 per cent in each of the 10 age bins in Fig. 9 as a function of the robust mean age of each bin including (left-hand panel, filled triangles) and excluding (right-hand panel, open triangles) the Hercules stream. As in N04, the youngest and oldest age bins have been excluded from the power-law fit to avoid biases due to unrelaxed young structures and thick disc stars, respectively.
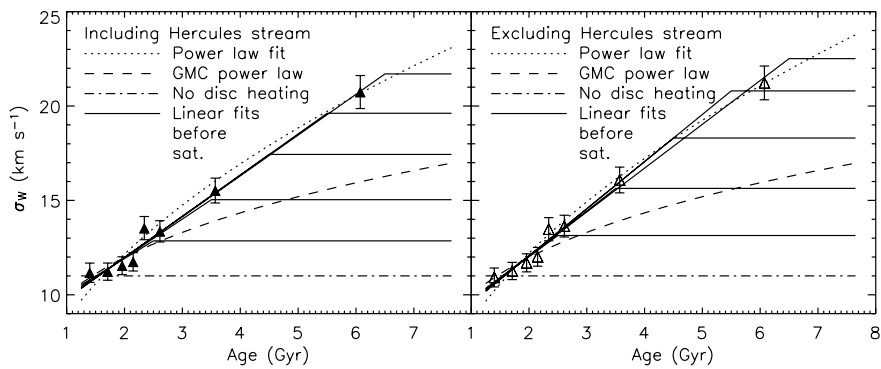
Figure 11. N04 linear age–σ_W relation: robust σ_W of N04 single stars with relative age errors <25 per cent in the eight age bins included in the power-law fit in Fig. 10 as a function of the robust mean age of each bin including (left-hand panel, filled triangles) and excluding (right-hand panel, open triangles) the Hercules stream. The dot-dashed lines are models representing no disc heating, where the constant saturation level is set by the dispersion in the youngest bin in Fig. 10. The solid lines are linear fits to each set of data points up to 2.5, 3.5, 4.5, 5.5 and 6.5 Gyr. Thereafter these models saturate at constant dispersions.

needs to be set by observations. We have plotted their power-law prediction in Fig. 10, setting $a = \sigma_0 = 10$ km s^{-1} so that at the youngest age included in the fits (1.25 Gyr), $\sigma_W \approx 10.6$ km s^{-1}.

The linear age–σ_W plane in Fig. 11 highlights the unequal spacing in age of the age bins as a result of the N04 procedure requiring the

same number of stars in each bin. The densely distributed age bins at the young end confirm the presence of an age–σ_W relation for the young thin disc. However, N04 do not consider whether any other models fit their data better than a power law. They assume a power law is the best-fitting model and interpret this as evidence of

Table 3. χ^2 goodness-of-fit test results between the N04 age-binning data and disc heating models in Fig. 11. n is the number of data points included in the model fit. n_c is the number of constraints on the model fit. The number of degrees of freedom is $\nu = n - n_c$. The χ^2 probability distribution function for ν degrees of freedom, $Q(\chi^2 \,|\, \nu)$, is the standard statistical significance of the χ^2 test $[Q(\chi^2 \,|\, \nu) = 1 - P(\chi^2 \,|\, \nu)]$. If $Q(\chi^2 \,|\, \nu) > 0.003$ $[P(\chi^2 \,|\, \nu) < 0.997]$, the data accept the model at the 3σ statistical significance level. If $Q(\chi^2 \,|\, \nu) < 0.003$ $[P(\chi^2 \,|\, \nu) > 0.997]$, the data reject the model at the 3σ statistical significance level.

Model	n	n_c	ν	Hercules	χ^2	χ^2/ν	$Q(\chi^2 \,|\, \nu)$	3σ significance
Power-law fit	8	2	6	Included	9.0	1.5	0.176	The data accept the model
				Excluded	4.8	0.8	0.571	The data accept the model
GMC power law	8	2	6	Included	41.5	6.9	10^{-7}	The data reject the model
				Excluded	49.6	8.3	10^{-7}	The data reject the model
No disc heating	8	1	7	Included	210.1	30.0	$<10^{-16}$	The data reject the model
				Excluded	230.3	32.9	$<10^{-16}$	The data reject the model
Linear fit before saturation at 2.5 Gyr	8	3	5	Included	103.1	20.6	$<10^{-16}$	The data reject the model
				Excluded	103.5	20.7	$<10^{-16}$	The data reject the model
Linear fit before saturation at 3.5 Gyr	8	3	5	Included	47.8	9.5	10^{-9}	The data reject the model
				Excluded	41.9	8.4	10^{-7}	The data reject the model
Linear fit before saturation at 4.5 Gyr	8	3	5	Included	19.0	3.8	0.002	The data reject the model
				Excluded	13.1	2.6	0.022	The data accept the model
Linear fit before saturation at 5.5 Gyr	8	3	5	Included	6.3	1.3	0.279	The data accept the model
				Excluded	2.7	0.5	0.752	The data accept the model
Linear fit before saturation at 6.5 Gyr	8	3	5	Included	5.8	1.2	0.322	The data accept the model
				Excluded	4.8	1.0	0.445	The data accept the model

continued disc heating throughout its lifetime. The relative age error of <25 per cent translates to sparse sampling of the old thin disc (two data points) and the thick disc (one data point). These are the only three age bins between 2.9 and 15.2 Gyr and only the former two bins are included in the power-law fit. Therefore, the power law is not as tightly constrained at the old end as it is at the young end.

We test N04's assumption that a power law is the best-fitting model by generating alternative time dependencies of disc heating models (overlaid in Fig. 11) and comparing them to the data. Our main aim is to establish whether the age–σ_W relation saturates for older stars. This means we are not so concerned with the exact functional form of the relation younger than a hypothetical saturation age. Thus we simply define models as linear fits of the data points up to a hypothetical saturation age, after which σ_W is constant with time, set by the σ_W at the hypothetical saturation age. The number of constraints on each power-law model fit (n_c) is 2 because the number of degrees of freedom (ν) is reduced by the two constraints of the fit: the slope and intercept. This is also the case for each linear fit before saturation model but ν is further reduced by one more constraint: the choice of saturation epoch. The χ^2 statistic for our purpose of comparing the observed distribution of σ_W to a model is

$$\chi^2 = \sum_{i=1}^{n} \left(\frac{\sigma_{W_i}^{O} - \sigma_{W_i}^{E}}{\Delta \sigma_{W_i}^{O}} \right)^2, \tag{4}$$

where $\sigma_{W_i}^{O}$ is the observed σ_W of the ith age bin, measured as a robust σ_W, and $\sigma_{W_i}^{E}$ is the robust σ_W expected according to a model.

As expected, Figs 10 and 11 show that the largest effect in removing the Hercules stream from the N04 binning sample is seen in the oldest thick disc age bin, which is not included in the age–σ_W relation. Excluding the Hercules stream stars removes Hercules

stream thin disc stars from the thick disc region of phase space and so the thick disc σ_W increases slightly. Figs 10 and 11 and Table 3 show that removing the Hercules stream has a negligible effect on the age–σ_W relation. This may suggest that there are insufficient numbers of Hercules stars in each age bin for the hypothetically higher Hercules σ_W to affect the relation. It also suggests that dynamical streams are well phase-mixed in W, supporting our argument that the age–σ_W relation can be constrained from the N04 data.

Table 3 shows that the N04 age-binned data (including the Hercules stream) accept the power law and thus halo black holes are not ruled out as vertical disc heating sources. As expected the data strongly reject a no disc heating model and linear fits before saturation at 2.5- and 3.5-Gyr models. The data also reject the GMC heating power law. However, the $Q(\chi^2 \,|\, \nu)$ values for this model are very sensitive to the initial σ_W. As mentioned earlier, if the unrelaxed early age bins actually have larger values of σ_W, then the Hänninen & Flynn (2002) model could perhaps be accepted by the data. We confirm one of N04's key results that disc heating does not saturate at an early stage. The linear fit before saturation at 4.5-Gyr model is only marginally rejected by the data including the Hercules stream, while the data excluding the Hercules stream accept this model. Models with linear fits before saturation at 5.5 and 6.5 Gyr are accepted by the data including and excluding the Hercules stream. Hence, the N04 data do not require a power law and actually statistically prefer saturation after $\sim$4.5 Gyr.

3.6 Higher resolution age binning

Higher resolution age binning is required to try to further rule out other disc heating models. Linear age binning, which needs bins of constant age range, will sample the old thin disc with more data
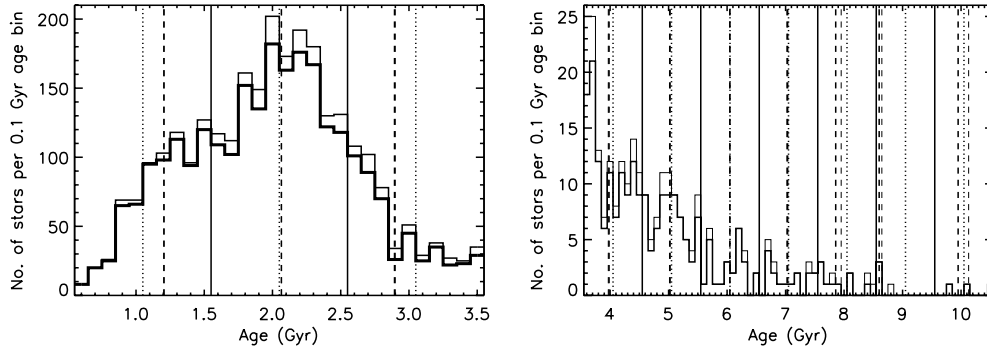
Figure 12. Discrete age distribution of the N04 single stars with absolute age errors <1 Gyr, split between the youngest three age bins (left-hand panel) and the oldest seven age bins (right-hand panel). The thin lines correspond to the whole sample and the thick lines are the subsample excluding the Hercules stream. Because the N04 catalogue stellar ages are provided to the nearest 0.1 Gyr, each 0.1-Gyr histogram bin only contains stars with the exact age that its histogram step is centred on, for example, the youngest histogram bin, centred on 0.6 Gyr, only contains stars with exactly 0.6 Gyr ages but the histogram step spans 0.55–0.65 Gyr. The vertical solid lines (including the vertical edges of the plots) are the boundaries to the age bins. The dotted lines are the central ages of each age bin. The robust mean ages within each age bin for the whole sample (thin-dashed lines) and subsample (thick-dashed lines) are indistinguishable until the three oldest age bins.
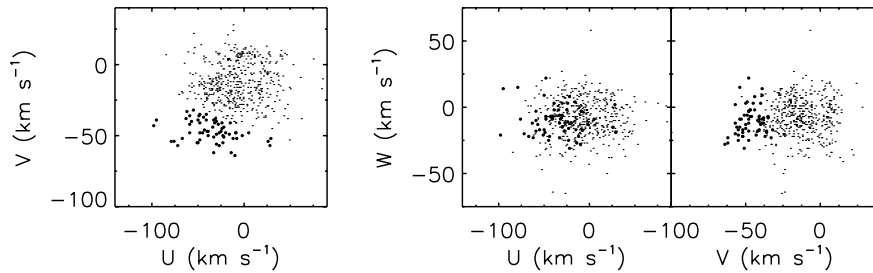
Figure 13. $U-V$ (left-hand panel), $U-W$ (middle panel) and $V-W$ (right-hand panel) space velocity diagrams of the 527 N04 single stars with absolute age errors <1 Gyr in the $2.5 <$ age $\leqslant 3.5$ Gyr age bin. We have assigned 62 N04 stars in this age bin to the Hercules stream (filled circles) using the Hercules stream UV phase space (defined by F05, see Fig. 3) and the Hercules stream W phase space (defined by F05, see Figs 4 and 5).
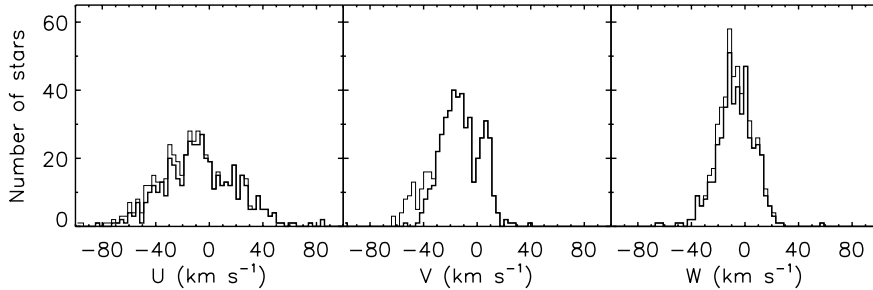
Figure 14. U (left-hand panel), V (middle panel) and W (right-hand panel) velocity distributions of the N04 single stars with absolute age errors <1 Gyr in the $2.5 <$ age $\leqslant 3.5$ Gyr age bin (thin line) and a subsample of these stars that excludes the Hercules stream (thick line), as defined in Figs 3–5.

points. Selecting the range of each age bin to be 1-Gyr wide more than doubles the number of data points sampling the old thin disc and thick disc. It also has more than half the number of age bins sampling the young thin disc but this regime has already been well constrained in the previous section.

We also chose an absolute age error of <1 Gyr so that any star can only shift laterally by a maximum of one age bin. This is not the case with the N04 binning. The preponderance of young stars in the N04 magnitude-limited sample (because of their higher luminosity) means their bins are more narrow than the typical age errors (<25 per cent) so the errors of some young stars span more than one age bin. Absolute age errors <1 Gyr means selecting stars with $\sigma_{age}^{high} -$ age < 1 Gyr and age $- \sigma_{age}^{low} < 1$ Gyr. Selecting single stars with absolute age errors <1 Gyr actually samples more stars

(3083) than the relative age error of <25 per cent (2801) because the vast majority of N04 stars are between 1- and 3-Gyr old (see N04's fig. 17). The youngest and oldest stars with an absolute age error <1 Gyr are 0.6 and 10.5 Gyr, constraining our age interval to $0.5 <$ age $\leqslant 10.5$ Gyr, giving us 10 1-Gyr-wide age bins. Fig. 12 shows the age distribution of our new sample.

Figs 13 and 14 show the space velocity diagrams and histograms, respectively, of a representative age bin from our new sample (plots of all our age bins are in Appendix A) that is most similar in age to the N04 age bin in Figs 1 and 2. Unlike the N04 binning in Fig. 2 (and Fig. A2), the age bin in Fig. 14 (and the two younger bins, all representing the young thin disc, in Fig. A4) do not suffer from statistical noise. They show the non-Gaussianity of the U and V distributions compared to W more clearly than in Figs 2 and A2.

Again, the young thin disc W histograms do not look completely relaxed. Fig. A4 clearly shows that only including stars with errors <1 Gyr severely reduces the numbers of stars in the older bins. The oldest W distribution that is still approximately a complete symmetric Gaussian and statistically significant with 26 stars is in bin 5.5 < age ⩽ 6.5 Gyr. Therefore, after the removal of statistically insignificant age bins older than 6.5 Gyr, our higher age resolution binning only adds one extra bin with which to constrain the age–σ_W relation of the old thin disc. The 5.5 < age ⩽ 6.5 Gyr is the oldest age bin included in the power-law fit in Fig. 15. The power-law fit to our binning produces a higher scaling (heating) exponent than the N04 binning power law: $k = 0.63 \pm 1.21$ including the Hercules stream ($k = 0.60 \pm 1.22$ excluding the Hercules stream).

We plot all the age bins from Fig. 12 in Fig. 15 but differentiate between the statistically significant and insignificant bins. Although not included in the power-law fit, the oldest age bin in N04's binning in Fig. 10 (and N04's fig. 31), seems to be a continuation of the power law, suggesting it is part of a continuing heating process. The oldest age bin includes some thick disc stars, which have been shown by many authors to have approximately double the thin disc σ_W. This thick disc signature is not seen in the N04 binning because the oldest age bin spans the oldest part of the thin disc and all the thick disc so it is numerically dominated by old thin disc stars that decrease σ_W. Our higher age resolution bins better resolve the thin disc–thick disc transition region. The age bins centred on 8 and 9 Gyr in Fig. 15 show a modest increase in σ_W compared to the power-law fits, reaching values more associated with the thick disc, 35 ± 3 km s^{-1} (Chiba & Beers 2000), 39 ± 4 km s^{-1} (Soubiran, Bienaymé & Siebert 2003), than the thin disc. This is in agreement with the jumps in the age–velocity dispersion relation at 8 and 9 Gyr found, respectively, by Sommer-Larsen & Antonuccio-Delogu (1993) and Quillen & Garnett (2001), the latter being significant at the 2–3σ level. The abrupt increase is interpreted as a formation signature of the thick disc, which is consistent with models where the thick disc was formed by dramatic disc heating when a satellite galaxy falls on to the Galactic disc in a minor merger ∼10 Gyr ago (Gilmore, Wyse & Kuijken 1989; Freeman 1991; Toth & Ostriker 1992; Quinn et al. 1993). Despite their statistical insignificance, it is tempting to associate these bins with the formation of the thick disc.

Again as expected, Figs 15 and 16 show that the largest effect in removing the Hercules stream from our binning sample is seen in the oldest thick disc age bins, which are not included in the age–σ_W relation. Figs 15, 16 and Table 4 show that removing the Hercules stream has a negligible effect on the age–σ_W relation, allowing the relation to be constrained by our age binning as well as the N04 binning.

The same disc heating models as before are considered with the results in Table 4. Again, we have plotted the GMC power law in
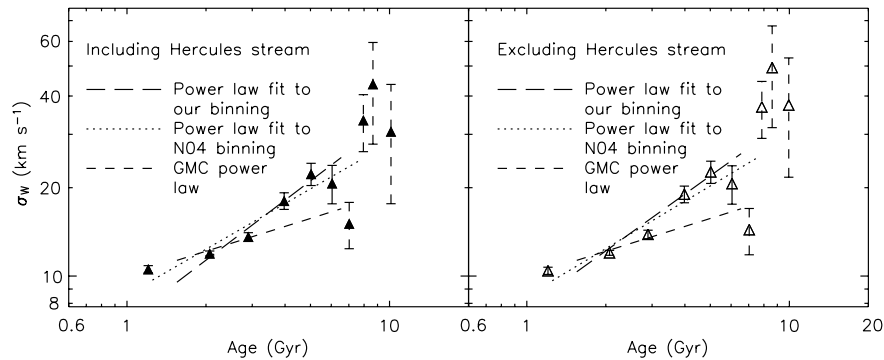
Figure 15. Our logarithmic age–σ_W relation: robust σ_W of N04 single stars with absolute age errors <1 Gyr in each of the 10 age bins in Fig. A4 as a function of the robust mean age of each bin including (left-hand panel, filled triangles) and excluding (right-hand panel, open triangles) the Hercules stream. As in N04, the youngest age bin has been excluded from our power-law fit (long-dashed line) to avoid biases due to unrelaxed young structures. The oldest age bin included in our fit is centred on 6 Gyr. Older age bins are excluded because they contain insufficient numbers of stars (see Fig. 12) for their σ_W values to be statistically significant (dashed error bars). The distribution of W velocities in the age bins centred on 10 Gyr do not yield robust values of σ_W. Therefore, their standard deviation is plotted instead.
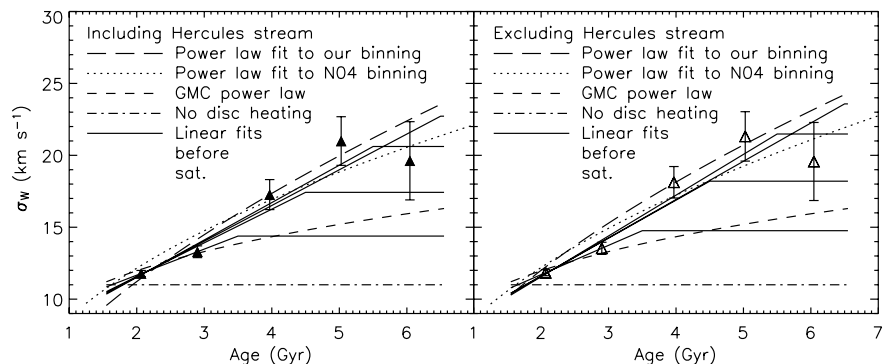
Figure 16. Our linear age–σ_W relation: robust σ_W of N04 single stars with absolute age errors <1 Gyr in the five age bins included in our power-law fit in Fig. 15 as a function of the robust mean age of each bin including (left-hand panel, filled triangles) and excluding (right-hand panel, open triangles) the Hercules stream. The dot–dashed lines are models representing no disc heating, where the constant saturation level is set by the dispersion in the youngest bin in Fig. 15. The solid lines are linear fits to each set of data points up to 2.5, 3.5, 4.5, 5.5 and 6.5 Gyr. Thereafter these models saturate at constant dispersions.

Table 4. χ^2 goodness-of-fit test results between our age-binning data and disc heating models in Fig. 16. n is the number of data points included in the model fit. n_c is the number of constraints on the model fit. The number of degrees of freedom is $\nu = n - n_c$. The χ^2 probability distribution function for ν degrees of freedom, $Q(\chi^2 \mid \nu)$, is the standard statistical significance of the χ^2 test $[Q(\chi^2 \mid \nu) = 1 - P(\chi^2 \mid \nu)]$. If $Q(\chi^2 \mid \nu) > 0.003$ $[P(\chi^2 \mid \nu) < 0.997]$, the data accept the model at the 3σ statistical significance level. If $Q(\chi^2 \mid \nu) < 0.003$ $[P(\chi^2 \mid \nu) > 0.997]$, the data reject the model at the 3σ statistical significance level.

Model	n	n_c	ν	Hercules	χ^2	χ^2/ν	$Q(\chi^2 \mid \nu)$	3σ significance
Our power-law fit	5	2	3	Included	8.5	2.8	0.037	The data accept the model
				Excluded	17.4	5.8	0.001	The data reject the model
N04 power-law fit	5	2	3	Included	17.7	4.4	0.001	The data reject the model
				Excluded	17.0	5.7	0.001	The data reject the model
GMC power law	5	2	3	Included	68.0	22.7	$<10^{-16}$	The data reject the model
				Excluded	28.4	9.5	10^{-6}	The data reject the model
No disc heating	5	1	4	Included	126.1	31.5	$<10^{-16}$	The data reject the model
				Excluded	140.9	35.2	$<10^{-16}$	The data reject the model
Linear fit before saturation at 3.5 Gyr	5	3	2	Included	26.6	13.3	10^{-6}	The data reject the model
				Excluded	27.2	13.6	10^{-6}	The data reject the model
Linear fit before saturation at 4.5 Gyr	5	3	2	Included	7.1	3.6	0.028	The data accept the model
				Excluded	6.2	3.1	0.045	The data accept the model
Linear fit before saturation at 5.5 Gyr	5	3	2	Included	3.5	1.7	0.175	The data accept the model
				Excluded	3.9	1.9	0.146	The data accept the model
Linear fit before saturation at 6.5 Gyr	5	3	2	Included	4.0	2.0	0.136	The data accept the model
				Excluded	4.7	2.3	0.097	The data accept the model

Figs 15 and 16, setting $a = \sigma_0 = 10$ km s^{-1} so that at the youngest age included in the fits (1.55 Gyr), $\sigma_W \approx 11.2$ km s^{-1}. With our binning there are fewer degrees of freedom, so the $Q(\chi^2 \mid \nu)$ values are generally smaller in Table 4 than in Table 3 for the N04 binning. Our binned data including the Hercules stream accept our power-law model but marginally reject it when the stream is excluded. Both including and excluding the Hercules stream in our binned data also marginally reject the N04 power-law fit, strongly reject a no disc heating model, reject the GMC power law (although as discussed earlier, this may not be conclusive), reject a linear fit before saturation at 3.5-Gyr model but accept models with linear fits before saturation at 4.5, 5.5 and 6.5 Gyr. Hence, our binning reinforces results from the previous section that the data do not require a power law and actually statistically prefer saturation at $\sim$4.5 Gyr.

4 DISCUSSION

This paper revisits the Galactic thin disc age–velocity dispersion relation. We show that dynamical streams complicate the U and V velocity distribution functions such that a straightforward dispersion is not an adequate parametrization of their distribution functions. This calls into question the appropriateness of power-law fits to the σ_U and σ_V relations with stellar age. It shows that observationally measured σ_U and σ_V can only be used to constrain in-plane disc heating models if the N04 sample can be kinematically decomposed (like in F05) so that only the smooth velocity ellipsoidal background is used, excluding the dynamical streams. Their strong presence in the solar neighbourhood may cast doubt on the applications of σ_U in determining the asymmetric drift, the extrapolating to zero σ_U to recover the V solar motion and the interpretation of the velocity ellipsoid dispersion axis ratios σ_V/σ_U, σ_W/σ_U and σ_W/σ_V. F05 have

already pointed out using their sample that the underlying velocity ellipsoid, after the removal of streams is not centred on the commonly accepted radial anticentre motion. Instead it is centred on $\langle U \rangle = -2.78 \pm 1.07$ km s^{-1}. Inclusion of the streams yields the commonly accepted value: $\langle U \rangle = -10.25 \pm 0.15$ km s^{-1}.

The age–σ_W relation can be constrained using the N04 data set because the dynamical streams are well phase-mixed in W, as illustrated by removal of the Hercules stream having no effect on the relation, which also suggests that the Galactic bar does not vertically heat the local disc. We do not find any signature of the stellar warp in the Galactic disc so we do not need to exclude any N04 stars from the age–σ_W relation on this basis, because they are all free from this potential source of σ_W bias.

We reproduce the N04 age–σ_W relation and confirm their finding that vertical disc heating does not saturate at an early stage (before $\sim$4.5 Gyr). Their logarithmic age binning naturally led them to fit a power law. However, they did not consider other disc heating models and so their conclusion was that the power-law fit was evidence that vertical disc heating is continuous throughout the lifetime of the thin disc. We have considered other disc heating models that saturate after different epochs. Our key new result is that a power law is not required by their data. A power-law fit is statistically similar to disc heating models which saturate after $\sim$4.5 Gyr (including and excluding the Hercules stream). These saturation model fits are consistent with the observational turnover at $\sim$5 Gyr found by Carlberg et al. (1985). Simulations of vertical disc heating solely from GMCs find $k = 0.26$ (Hänninen & Flynn 2002). Figs 11 and 16 show that this power law is consistent with a minimal increase in σ_W for old stars, not too dissimilar to the models that saturate after 3.5 and 4.5 Gyr.

To see if the data could rule out any of the disc heating models considered, we examined the relation at a higher age resolution

but found very similar results to the N04 age binning. Therefore, two diametrically different age-binning methods using the best data available for constraining the age–σ_W relation still cannot distinguish between competing disc heating models. The issue is unlikely to be resolved until there are many more space velocities and ages measured for old thin disc stars. This may need to wait until the ESA *Gaia* satellite era (Perryman et al. 2001).

Nevertheless, our results provide new constraints to be fulfilled by disc heating simulations. Prior to this paper, new disc heating simulations would have tried to explain the continued disc heating found in all three cardinal directions by N04. Now, we have shown that new simulations cannot use in-plane age–velocity dispersion relations derived using stellar samples containing dynamical streams and straightforward dispersions. Also, the new simulations must be able to reproduce the complex U and V substructure in the solar neighbourhood, caused by dynamical streams, while modelling in-plane disc heating mechanisms (e.g. De Simone et al. 2004). They must also take into account that these dynamical streams dominate the solar neighbourhood velocity distribution function and include evaporating star clusters, which may have been created by the spiral wave that spawned the streams.

Assuming our choice of initial σ_W and the modelling of Hänninen & Flynn (2002) are both realistic, simulations of vertical disc heating solely from GMCs appear unable to reproduce the amplitude of our age–σ_W relation on their own. This suggests that another vertical disc heating mechanism is or has been involved in the evolution of the Galactic thin disc. We have shown that the data do not rule out heating by halo black holes. However, this option has no observational support. Black holes passing through the disc would probably reveal themselves as high proper motion X-ray sources and no such objects have been found.

In the context of the hierarchical galaxy formation paradigm, another vertical heating mechanism is minor mergers with dwarf galaxies. We find extremely tentative evidence of an abrupt feature in the age–σ_W relation at $\sim$8 Gyr, which could be the sudden vertical heating of an early thin disc into the thick disc due to a major merger (Quinn et al. 1993). The relation does not exhibit any other strong features like this, suggesting it is unlikely that the Milky Way suffered another major merger in the last $\sim$8 Gyr but it does not rule out minor mergers during this period of relatively quiescent disc evolution. In Figs 11 and 16, the old thin disc bins with σ_W greater than the GMC power law may be the signature of minor mergers that took place $\gtrsim$3 Gyr ago at redshift $\gtrsim$0.5. Velazquez & White (1999) showed that disc galaxies can accrete quite massive satellites without destroying the disc, particularly if the orbits are retrograde. They found that a satellite on a retrograde orbit with an initial mass of 20 per cent of the Milky Way's disc could increase the velocity ellipsoid at the solar neighbourhood by $\Delta\sigma_W = 6\,\mathrm{km\,s^{-1}}$. The same satellite, but on a prograde orbit, leads to $\Delta\sigma_W = 12\,\mathrm{km\,s^{-1}}$. It is intriguing that the difference between the observed age–σ_W relation and the predicted relation only heated by GMCs is $\sim$6 km s^{-1} at an epoch $\sim$5 Gyr ago in Fig. 16. The agreement between the observed age–σ_W relation and the predicted relation only heated by GMCs is good between the present day and $\sim$3 Gyr ago, which may suggest that no minor mergers with significant satellite mass have occurred in the last $\sim$3 Gyr.

The RAdial Velocity Experiment (RAVE; Steinmetz et al. 2006) is measuring the radial velocities of stars further from the Sun than the N04 and F05 samples. RAVE vertical velocities can be used to test the vertical smoothness of the velocity distribution further from the Galactic plane than possible with N04 and F05, as well as to search for tidal streams falling on to the Milky Way disc from satellite galaxies (Seabroke et al., 2007), which may be responsible for some of the vertical disc heating observed in the age–σ_W relation in the solar neighbourhood.

REFERENCES

Alonso A., Arribas S., Martinez-Roger C., 1996, A&A, 313, 873
Baranne A., Mayor M., Poncet J. L., 1979, Vistas Astron., 23, 279
Barbanis B., Woltjer L., 1967, ApJ, 150, 461
Bensby T., Oey M. S., Feltzing S., Gustafsson B., 2007, ApJ, 655, L89
Brown A. G. A., Arenou F., van Leeuwen F., Lindegren L., Luri X., 1997, in ESA Special Publication, Vol. 402, Hipparcos-Venice 97. ESA Publications Division, Noordwijk, p. 63
Carlberg R. G., Sellwood J. A., 1985, ApJ, 292, 79
Carlberg R. G., Dawson P. C., Hsu T., Vandenberg D. A., 1985, ApJ, 294, 674
Carr B. J., Lacey C. G., 1987, ApJ, 316, 23
Chiba M., Beers T. C., 2000, AJ, 119, 2843
Crawford D. L., 1975, AJ, 80, 955
De Simone R., Wu X., Tremaine S., 2004, MNRAS, 350, 627
Dehnen W., 1998, AJ, 115, 2384
Dehnen W., 1999, ApJ, 524, L35
Dehnen W., 2000, AJ, 119, 800
Dehnen W., Binney J. J., 1998, MNRAS, 298, 387
Edvardsson B., Andersen J., Gustafsson B., Lambert D. L., Nissen P. E., Tomkin J., 1993, A&A, 275, 101
ESA 1997, The *Hipparcos* Catalogue, ESA SP-1200
Famaey B., Jorissen A., Luri X., Mayor M., Udry S., Dejonghe H., Turon C., 2005, A&A, 430, 165 (F05)
Famaey B., Pont F., Luri X., Udry S., Mayor M., Jorissen A., 2007, A&A, 461, 957
Freeman K. C., 1991, in Sundelius B., ed., Dynamics of Disc Galaxies Göteborgs Univ. Göteberg, p. 15
Fuchs B., Dettbarn C., Wielen R., 1994, in Gurzadyan V. G., Pfenniger D., eds, Lecture Notes in Physics, Vol. 430, Ergodic Concepts in Stellar Dynamics. Springer-Verlag, Berlin, p. 34
Fux R., 2001, A&A, 373, 511
Gilmore G., Wyse R. F. G., Kuijken K., 1989, ARA&A, 27, 555
Girardi L., Bressan A., Bertelli G., Chiosi C., 2000, A&AS, 141, 371
Gomez A., Grenier S., Udry S., Haywood M., Meillon L., Sabas V., Sellier A., Morin D., 1997, in ESA Special Publication, Vol. 402, Hipparcos-Venice 97. ESA Publications Division, Noordwijk, p. 621
Hänninen J., Flynn C., 2002, MNRAS, 337, 731
Haywood M., 2002, MNRAS, 337, 151
Høg E. et al., 2000, A&A, 355, L27
Holmberg J., Nordström B., Andersen J., 2006, Mem. Soc. Astron. Ital., 77, 1065
Huang S., Carlberg R. G., 1997, ApJ, 480, 503
Jenkins A., 1992, MNRAS, 257, 620
Jenkins A., Binney J., 1990, MNRAS, 245, 305
Jørgensen B. R., Lindegren L., 2005, A&A, 436, 127
Kalnajs A. J., 1991, in Sundelius B., ed., Dynamics of Disc Galaxies. Göteborgs Univ., Göteborg, p. 323
Kroupa P., 2002, MNRAS, 330, 707
Lacey C. G., 1984, MNRAS, 208, 687
Lacey C. G., Ostriker J. P., 1985, ApJ, 299, 633
Luri X., Mennessier M. O., Torra J., Figueras F., 1996, A&AS, 117, 405
Mayor M., 1985, in Philip A. G. D., Latham D. W., eds, IAU Colloq. 88, Stellar Radial Velocities. L. Davis Press, Schenectady, p. 21

Ng Y. K., Bertelli G., 1998, A&A, 329, 943

Nordström B. et al., 2004, A&A, 418, 989 (N04)

Olsen E. H., 1983, A&AS, 54, 55

Olsen E. H., 1984, A&AS, 57, 443

Olsen E. H., 1988, A&A, 189, 173

Olsen E. H., 1993, A&AS, 102, 89

Olsen E. H., 1994a, A&AS, 104, 429

Olsen E. H., 1994b, A&AS, 106, 257

Perryman M. A. C. et al., 2001, A&A, 369, 339

Quillen A. C., 2003, AJ, 125, 785

Quillen A. C., Garnett D. R., 2001, in Funes J. G., Corsini E. M., eds, ASP Conf. Ser. Vol. 230, Galaxy Discs and Disc Galaxies: The Saturation of Disc Heating in the Solar Neighborhood and Evidence for a Merger 9 Gyr Ago. Astron. Soc. Pac., San Francisco, p. 87

Quillen A. C., Minchev I., 2005, AJ, 130, 576

Quinn P. J., Hernquist L., Fullagar D. P., 1993, ApJ, 403, 74

Reid I. N., Turner E. L., Turnbull M. C., Mountain M., Valenti J. A., 2007, ApJ, 665, 767

Salasnich B., Girardi L., Weiss A., Chiosi C., 2000, A&A, 361, 1023

Schuster W. J., Nissen P. E., 1989, A&A, 221, 65

Seabroke G. M. et al., 2007, MNRAS, submitted

Sellwood J. A., Binney J. J., 2002, MNRAS, 336, 785

Sellwood J. A., Carlberg R. G., 1984, ApJ, 282, 61

Skuljan J., Hearnshaw J. B., Cottrell P. L., 1999, MNRAS, 308, 731

Sommer-Larsen J., Antonuccio-Delogu V., 1993, MNRAS, 262, 350

Soubiran C., Bienaymé O., Siebert A., 2003, A&A, 398, 141

Spitzer L. J., Schwarzschild M., 1951, ApJ, 114, 385

Spitzer L. J., Schwarzschild M., 1953, ApJ, 118, 106

Steinmetz M. et al., 2006, AJ, 132, 1645

Stromgren B., 1987, in Gilmore G., Carswell B., eds, NATO ASIC Proc. 207, The Galaxy. D. Reidel Publishing Co., Dordrecht, p. 229

Toth G., Ostriker J. P., 1992, ApJ, 389, 5

Valenti J. A., Fischer D. A., 2005, ApJS, 159, 141

Velazquez H., White S. D. M., 1999, MNRAS, 304, 254

Villumsen J. V., 1985, ApJ, 290, 75

Walker I. R., Mihos J. C., Hernquist L., 1996, ApJ, 460, 121

Wielen R., 1977, A&A, 60, 263

Woolley R., 1961, The Observatory, 81, 203

# APPENDIX A: SPACE VELOCITY DISTRIBUTIONS IN ALL THE AGE BINS

A1 N04 age bins

For completeness, all the N04 age bins have their space velocity diagrams plotted in Fig. A1 and their space velocity histograms plotted in Fig. A2.

A2 Our age bins

For completeness, all our age bins have their space velocity diagrams plotted in Fig. A3 and their space velocity histograms plotted in Fig. A4.
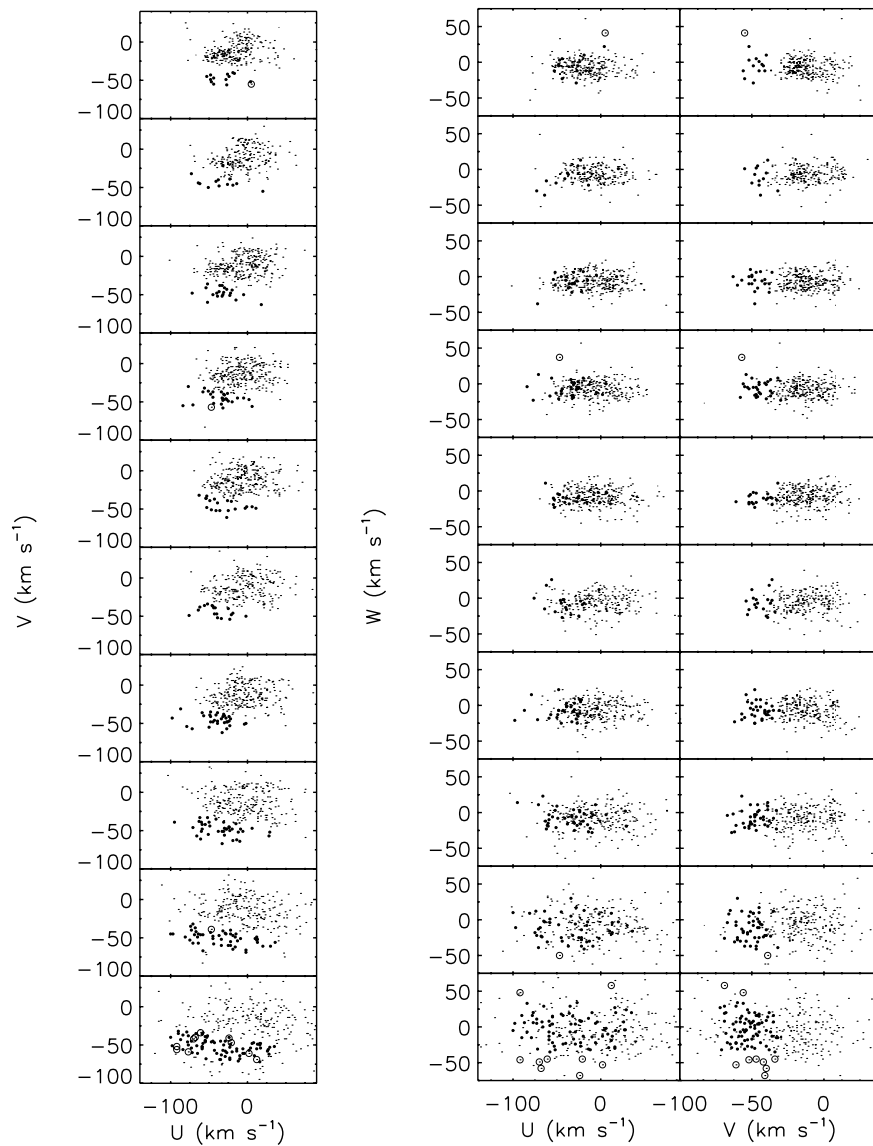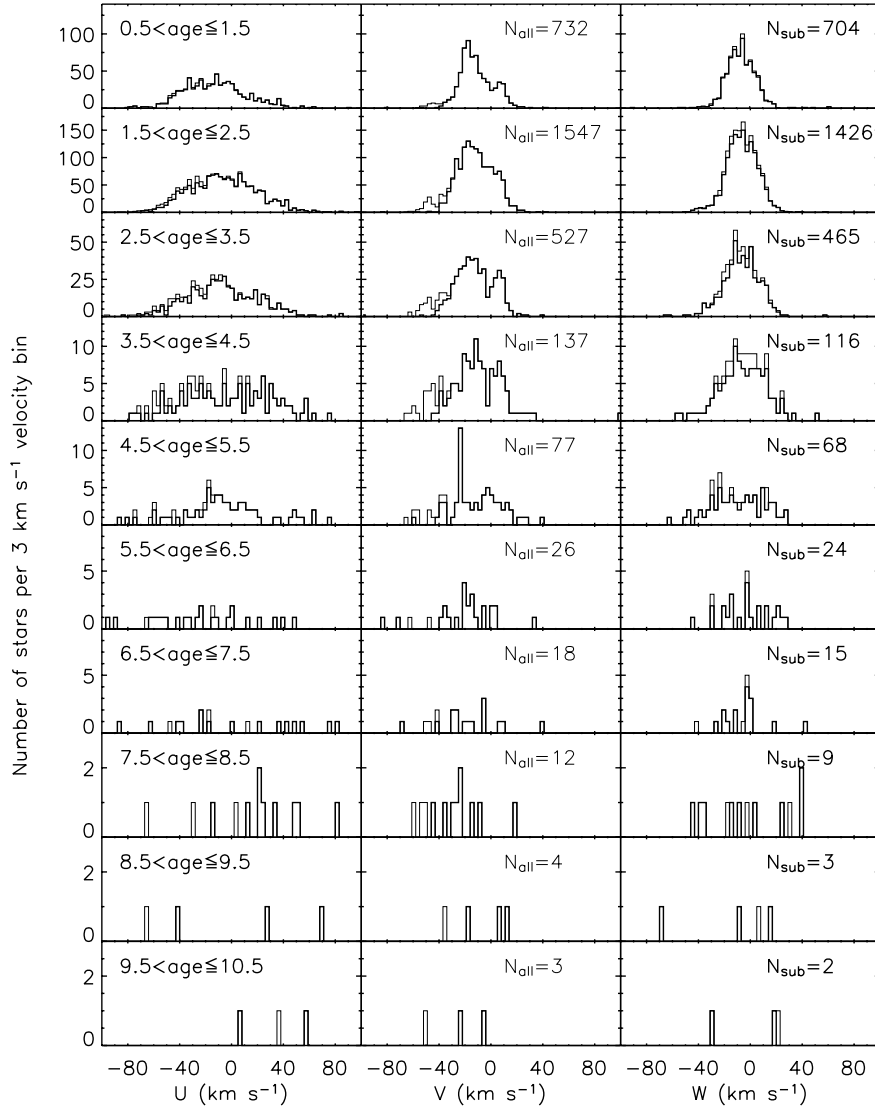

Figure A1. $U-V$ (left-hand panels), $U-W$ (middle panels) and $V-W$ (right-hand panels) space velocity diagrams of the 278 N04 single stars with relative age errors <25 per cent plotted in the 10 age bins from Fig. 9 (youngest at the top and oldest at the bottom). We have assigned N04 stars to the Hercules stream (filled circles) and high-velocity stars (open circles) in the Hercules stream UV phase space (defined by F05, see Fig. 3) but outside the Hercules stream W phase space (defined by F05, see Figs 4 and 5).
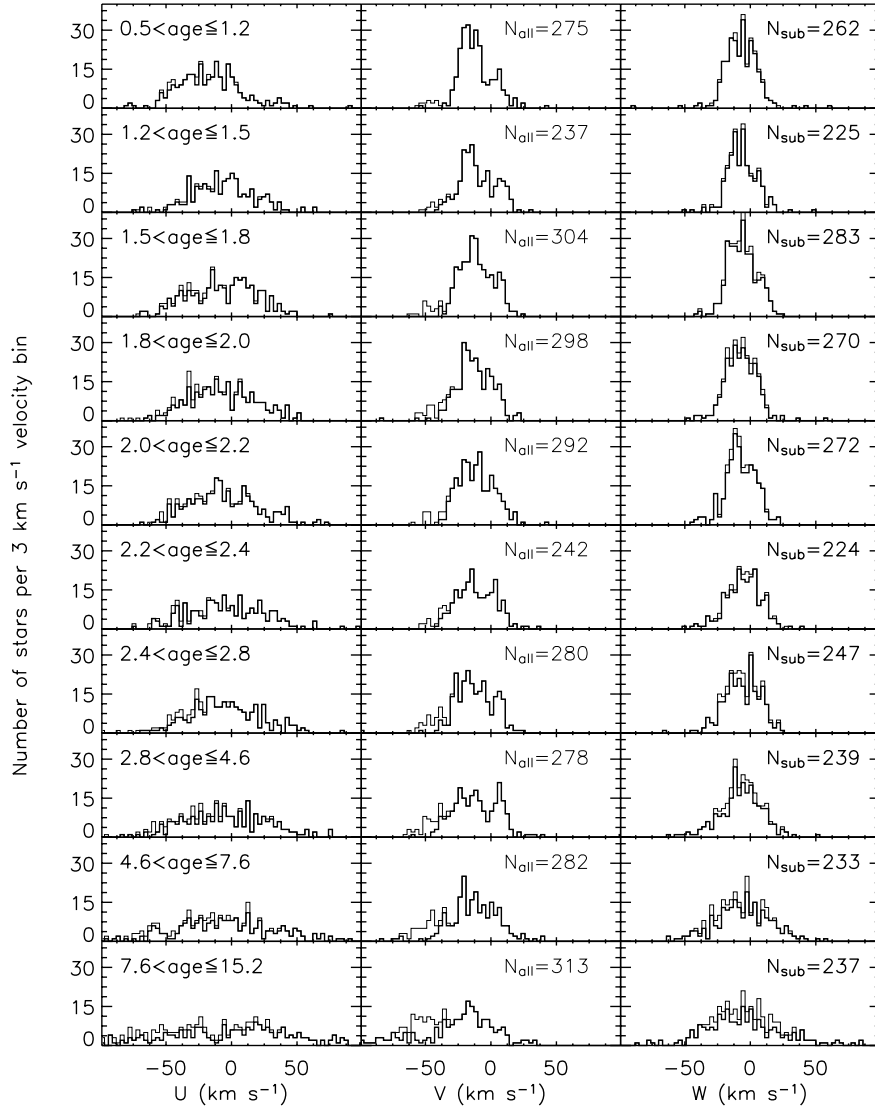
Figure A2. *U* (left-hand panels), *V* (middle panels) and *W* (right-hand panels) velocity distributions of the N04 single stars with relative age errors <25 per cent plotted in the 10 age bins that dissect their corresponding age distribution to give approximately equal numbers (N_{all}) of stars in each age bin (thin lines) and a subsample (N_{sub}) of these stars that excludes the Hercules stream (as defined in Figs 3–5) plotted in the same age bins (thick lines). The boundaries of each age bin are given in Gyr.
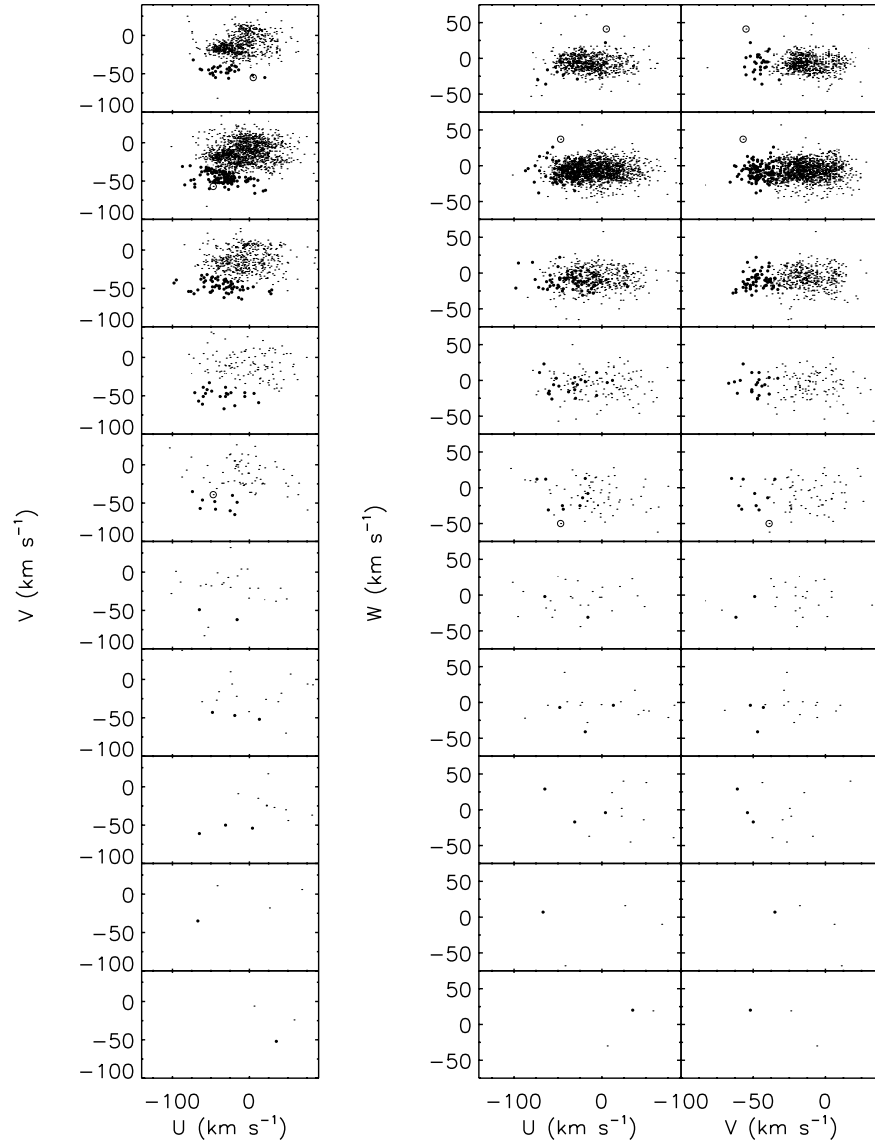
Figure A3. $U-V$ (left-hand panels), $U-W$ (middle panels) and $V-W$ (right-hand panels) space velocity diagrams of the N04 single stars with absolute age errors <1 Gyr plotted in the 10 age bins from Fig. 12 (youngest at the top and oldest at the bottom). We have assigned N04 stars to the Hercules stream (filled circles) and high-velocity stars (open circles) in the Hercules stream *UV* phase space (defined by F05, see Fig. 3) but outside the Hercules stream *W* phase space (defined by F05, see Figs 4 and 5).

Figure A4. *U* (left-hand panels), *V* (middle panels) and *W* (right-hand panels) velocity distributions of the N04 single stars with absolute age errors <1 Gyr plotted in the 10 age bins that dissect their corresponding age distribution to give equal width (1 Gyr) age bins. The boundaries of each age bin are given in Gyr. N_{all} is the total number of stars in each age bin (thin lines) and N_{sub} is the number of these stars in the subsample that excludes the Hercules stream (as defined in Figs 3–5) plotted in the same age bins (thick lines).

This paper has been typeset from a TEX/LATEX file prepared by the author.